

# Functional renormalisation group approach to shell models of turbulence

Côme Fontaine<sup>1</sup>, Malo Tarpin<sup>2</sup>, Freddy Bouchet<sup>2</sup>, and Léonie Canet<sup>1,3\*</sup>

<sup>1</sup> Univ. Grenoble Alpes, CNRS, LPMMC, 38000 Grenoble, France

<sup>2</sup> ENS Lyon, 69000 Lyon, France

<sup>3</sup> Institut Universitaire de France, 75000 Paris, France

\* leonie.canet@grenoble.cnrs.fr

## Abstract

Shell models are simplified models of hydrodynamic turbulence, retaining only some essential features of the original equations, such as the non-linearity, symmetries and quadratic invariants. Yet, they were shown to reproduce the most salient properties of developed turbulence, in particular universal statistics and multi-scaling. We set up the functional renormalisation group formalism to study generic shell models. Focusing on the Sabra shell model, we obtain the renormalisation group fixed-point describing its universal properties for a forcing exerted at large scales. We find that the structure functions exhibit universal scaling, and show that they acquire anomalous scaling exponents, with  $\zeta_2 \simeq 0.74 \pm 0.02$ , which is in good agreement with results from numerical simulations. Moreover, we study the influence of a long-range power-law forcing, and resolve its interplay with the Sabra fixed-point corresponding to large scale forcing.

---

## Contents

<b>1</b>	<b>Introduction</b>	<b>2</b>
<b>2</b>	<b>Sabra shell model and field theory</b>	<b>4</b>
2.1	Sabra shell model	4
2.2	Path integral formalism	6
<b>3</b>	<b>Functional renormalisation group formalism</b>	<b>7</b>
3.1	General framework for shell models	7
3.2	General form of the propagator	9
3.3	Approximation schemes in FRG	10
<b>4</b>	<b>Fixed point and anomalous exponents</b>	<b>11</b>
4.1	Leading order approximation	11
4.2	Fixed-point solution	12
4.3	Structure functions	13
4.3.1	Second order structure function	13
4.3.2	Third order structure function	14
4.3.3	Higher order structure functions	15

<b>5</b>	<b>Effect of long-range forcing</b>	<b>17</b>
5.1	Long-range forcing in the FRG framework	17
5.2	Purely long-range fixed-point	18
5.3	Interplay between the LR and SR fixed-points	20
5.4	Dissipative range and thermal noise	20
<b>6</b>	<b>Conclusion and perspectives</b>	<b>21</b>
<b>A</b>	<b>Sabra model in the presence of the zero mode</b>	<b>22</b>
<b>B</b>	<b>FRG flow equations in the LO approximation</b>	<b>24</b>
<b>C</b>	<b>Numerical integration of the flow equations</b>	<b>25</b>
<b>D</b>	<b>Dependence on the regulator</b>	<b>26</b>
<b>E</b>	<b>Structure functions of higher order</b>	<b>27</b>
<b>F</b>	<b>Constraints from translational invariance on 4-point configurations</b>	<b>29</b>
	<b>References</b>	<b>31</b>

---

## 1 Introduction

Hydrodynamic turbulence is a multi-scale non-linear phenomenon which still lacks a complete theoretical understanding. One of the salient stumbling blocks is the calculation of intermittency effects [1]. An homogeneous and isotropic three-dimensional (3D) turbulent flow exhibits at large Reynolds number (Re) universal properties for scales in the inertial range, that is away from the large scale  $L$  where the forcing is exerted and from the Kolmogorov scale  $\eta$  where dissipation occurs. In this range, empirical evidence suggests that the structure functions  $S_p(r)$  of velocity increments behave as power-laws

$$S_p(r) = \left\langle \left| \mathbf{v}(t, \mathbf{x} + \mathbf{r}) - \mathbf{v}(t, \mathbf{x}) \right|^p \right\rangle \sim r^{\zeta_p}, \quad r = |\mathbf{r}|, \quad (1)$$

with universal exponents  $\zeta_p$  which are independent of the forcing mechanism. Kolmogorov established in his celebrated 1941 theory (K41) [2, 3] the exact result  $\zeta_3 = 1$  in the limit of infinite Re. Then assuming self-similarity in the statistical sense, he inferred  $\zeta_p = p/3$ . However, the statistics of real turbulent flows do not obey K41 theory. Accumulated evidence from experiments and numerical simulations shows that the structure functions exhibit anomalous scaling with exponents  $\zeta_p \neq p/3$ , which reveals the multi-scale or multi-fractal nature of developed turbulence [1]. The deviations from K41 theory are referred to as intermittency effects, and their calculation from Navier-Stokes equation remains an unsolved problem.

Rather than directly tackling the Navier-Stokes equation, a fruitful alternative approach to gain insights in the statistical properties of turbulence is to conceive simplified models, which involve a considerably reduced number of degrees of freedom. Among such models are the one-dimensional

Burgers equation [4], the Constantin-Lax-Majda model [5], or shell models [6, 7]. Shell models, originally introduced by Gledzer [8], Desnyansky and Novikov [9] are inspired by the energy cascade picture, and are formulated as an Euler-like dynamics of a few Fourier modes  $v(t, k_n)$  of the velocity field whose wave-numbers are logarithmically spaced:  $k_n = k_0 \lambda^n$  with  $\lambda > 1$ . For simplicity,  $v$  and  $k_n$  are simply taken as scalars rather than three-dimensional vectors, such that the geometry is lost, and they do not correspond to an exact projection of the Navier-Stokes equation [10–12]. Yet, they preserve the features of the dynamical equations which are intuitively thought as important, such as the structure of the quadratic non-linearity, symmetries, quadratic invariants. Indeed, they were shown to generate multi-scaling, and for some values of the parameters they even quantitatively reproduce the anomalous exponents measured in hydrodynamic turbulence [13–15]. This was numerically demonstrated in particular for the Gledzer-Yamada-Ohkitani (GOY) shell model [8, 13], and its improved version proposed by L’vov *et al* called the Sabra model [15]. The latter allows for efficient and more accurate numerical determination of the anomalous exponents by suppressing some oscillatory behaviour of the original GOY model. One can also derive analytical results on intermittency for some specific models, such as the spherical shell model in the large  $N$  limit [16, 17], or shell models with a Hamiltonian structure [18] or specifically designed solvable models [19]. Note that one can also rigorously construct shell models which preserve the exact form of the original equation of motions [12].

However, for the GOY and Sabra models whose properties most closely resemble the ones of hydrodynamic turbulence, there is no analytical result on their anomalous scaling exponents. The calculation of anomalous exponents requires in general elaborated methods, such as the Renormalisation Group (RG), conceived by Wilson [20], which has been pivotal to understand the emergence of universality and to compute anomalous critical exponents associated with equilibrium second-order phase transitions. The idea of applying RG techniques to turbulence dates back to the early eighties [21–23] but has been thwarted by the absence of a small parameter to control perturbative expansions [24–26]. Since then, the formulation of the RG has deeply evolved, and matured into a very versatile and powerful framework, which allows for functional and non-perturbative implementations of the RG procedure (we refer to [27–30] for general reviews on FRG). In turbulence, the FRG has yielded two important results. The first one is the existence of the RG fixed-point which describes developed turbulence for a forcing concentrated at large scale, which is the relevant case for physical situations [31–33]. This fixed-point yields the exact four-fifth law and allows for the accurate computation of the Kolmogorov constant [34]. The second and prominent result derived from FRG is the expression of the general spatio-temporal dependence of multi-point multi-time Eulerian correlations [35]. This expression is exact in the limit of large wave-numbers, and provides not only the general form of the correlations, but also the associated constants. These predictions were quantitatively confirmed in direct numerical simulations for the two-point and three-point correlation functions [36, 37], and also for passive scalar turbulence [38, 39].

For shell models, despite some early attempts [40], the existence of a fixed-point describing their universal properties has been only postulated, but never demonstrated. In this paper, we employ FRG methods to study the shell models and, focusing on the Sabra model, we obtain the associated fixed-point for large-scale forcing. This allows us to explicitly access universal properties of the turbulent state. We consider in particular the structure functions of order  $p = 2, 3, 4, 5$ , that we calculate within an approximation called LO (leading order). Our central result is that this fixed-point yields anomalous scaling, in particular  $\zeta_2 \simeq 0.74 \pm 0.02$ , which is in quantitative agreement with the numerical value for the Sabra model [15]. Within the simple LO approximation, the exponents  $\zeta_p$  are anomalous, *i.e.* they differ from K41 scaling, but they are uni-fractal,

akin in a  $\beta$ -model [41]. A non-linear (multi-fractal) scaling is expected to emerge at the next level of approximation, not computed in this work.

The FRG framework also allows us to study the effect of a forcing which is not concentrated on the large scale but rather has an algebraic dependence on the scale. We refer to such forcing as long-range (implied in scale) throughout the paper, while a forcing concentrated on the large scale is referred to as short-range. Explicitly, a long-range forcing for shell models has a spectrum of the form  $N(k_n) \sim k_n^{-\rho}$ . In usual perturbative implementation of the RG for three-dimensional hydrodynamic turbulence, one considers a long-range forcing with a power-law spectrum  $N(k) \sim k^{4-d-\epsilon}$  in order to artificially introduce the expansion parameter  $\epsilon$  [22–26]. However, the interesting physical case corresponds to the uncontrolled limit  $\epsilon \rightarrow 4$ . This raises the question of whether the actual short-range fixed-point, corresponding to a large scale forcing, can be captured by such an expansion. This issue has been investigated in 3D numerical simulations with inconclusive results [42, 43], and revisited in a shell model [44]. Our FRG analysis shows that the long-range and short-range forcings yield two distinct fixed-points. In particular, the long-range fixed-point has normal scaling, whereas the short-range one is anomalous, and they do not coincide even in the limit where  $\rho \rightarrow 0$  (which is equivalent to  $\epsilon \rightarrow 4$  for 3D turbulence). It follows that anomalous intermittency exponents cannot be computed from taking the limit  $\rho \rightarrow 0$  of the long-range fixed-point. This provides a tangible indication that this is also the case for hydrodynamic turbulence.

The rest of the paper is organised as follows. The Sabra shell model and its key properties are reviewed in Sec. 2. We then use the path integral formalism to derive the field theory for shell models. In Sec. 3, we introduce the functional renormalisation group and how it can be implemented for the Sabra model, and we present the LO approximation studied in this work. The corresponding RG flow equations are derived and solved in Sec. 4. We show the existence of a fixed-point, and compute the structure functions and their anomalous exponents. Sec. 5 is devoted to the study of the long-range forcing and its interplay with the short-range fixed-point.

## 2 Sabra shell model and field theory

### 2.1 Sabra shell model

The Sabra shell model describes the dynamics of a set of complex amplitudes  $(v_n(t))_{n \in \mathbb{Z}}$ , which represent Fourier modes of the velocity in shells of wave-numbers  $k_n = k_0 \lambda^n$  with  $\lambda > 1$ . The time evolution of these amplitudes is given by a set of non-linear coupled ordinary differential equations [15]:

$$\begin{cases} \partial_t v_n = B_n[v, v^*] - \nu k_n^2 v_n + f_n \\ B_n[v, v^*] = i [a k_{n+1} v_{n+2} v_{n+1}^* + b k_n v_{n+1} v_{n-1}^* - c k_{n-1} v_{n-1} v_{n-2}] \end{cases}, \quad (2)$$

where  $\nu$  is the viscosity and  $f_n$  a forcing to maintain a turbulent stationary state. The three parameters  $a, b, c$  must satisfy the constraint  $a + b + c = 0$  to ensure that the inviscid ( $\nu = 0$ ) and unforced ( $f = 0$ ) version of (2) formally conserves two quadratic invariants. These are the total energy and total ‘‘helicity’’ (in analogy with 3D hydrodynamic turbulence), defined respectively as

$$E = \sum_n v_n v_n^*, \quad H = \sum_n \left(\frac{a}{c}\right)^n v_n v_n^*. \quad (3)$$

Since the equations can be rescaled to set one of the parameters to unity, and another one is fixed by the conservation constraint, we conform to the conventional choice of setting  $a = 1$

and  $b = -(1 + c)$ . Note that usually, shell models are defined for  $n \in \mathbb{N}$ , considering  $v_n = 0$  for all  $n < 0$ , which prescribes the boundary condition. Here, we consider  $n \in \mathbb{Z}$ , the negative indices corresponding to  $k_n \rightarrow 0$ . One may also define this shell model on a wave-number space containing the zero mode, which is discussed in Appendix A.

The model (2) possesses four symmetries, which are the invariance under time translations, space translations, time dilatations and discrete space dilatations. Since  $(v_n(t))_{n \in \mathbb{Z}}$  represents a sequence of Fourier modes, the translations in space correspond to phase shifts of the form  $v_n \rightarrow v'_n = e^{i\theta_n} v_n$ . The Sabra shell model is invariant under these shifts provided that the phases  $(\theta_n)_{n \in \mathbb{Z}}$  satisfy the recurrence relation  $\theta_{n+2} = \theta_{n+1} + \theta_n$ . The solutions of this equation are of the form

$$\theta_n = \frac{1}{\sqrt{5}} [\theta_0(\varphi_+ \varphi_-^n - \varphi_- \varphi_+^n) + \theta_1(\varphi_+^n - \varphi_-^n)], \quad (4)$$

where  $\varphi_{\pm} = (1 \pm \sqrt{5})/2$  are the solutions of  $\varphi^2 = 1 + \varphi$ . As shown in Ref. [15], the independence of the field configurations with respect to  $\theta_0, \theta_1$  implies that they must satisfy a rule of conservation of a quasi-momentum  $\kappa_n = \pm \varphi^n$ , which is that “the sum of incoming quasi-momenta (associated with a  $v$ ) is equal to the sum of outgoing quasi-momenta (associated with a  $v^*$ )”, as stated in [15]. This was early identified as a key advantage of the Sabra shell model compared to the GOY one. Indeed, it is natural to assume that the statistics of the model respect this symmetry. The conservation of the quasi-momentum then entails strict constraints on the non-vanishing field configurations, contrarily to the law of conservation of momentum for the Fourier transform in the continuum space.

The analogy with Fourier modes should not be pushed too far nonetheless. Indeed, in shell models, the shell variables  $v_n$  are rather surrogates for the velocity increments in 3D hydrodynamical turbulence and as such their moments are the analogues of the structure functions. For  $p = 2$  and  $p = 3$ , the only structure functions compatible with the conservation of the quasi-momentum are:

$$S_2(k_n) = \langle v_n v_n^* \rangle \quad (5)$$

$$S_3(k_n) = \text{Im} \langle v_{n+1}^* v_n v_{n-1} \rangle. \quad (6)$$

For higher orders  $p$ , one defines the following structure functions:

$$S_p(k_n) = \begin{cases} \langle |v_n|^p \rangle & \text{if } p \text{ is even} \\ \text{Im} \langle v_{n+1}^* v_n v_{n-1} |v_n|^{p-3} \rangle & \text{if } p \text{ is odd.} \end{cases} \quad (7)$$

The great interest of the GOY and Sabra shell models is that these structure functions exhibit a very similar behaviour as in hydrodynamic turbulence. At high Reynolds number (large scale forcing and small viscosity  $\nu$ ), they display an inertial range of shell indices with universal scaling laws characterised by anomalous exponents [6, 7, 15]. For the Sabra model, all structure functions behave as:

$$S_p(k_n) = C_p \left( \frac{\varepsilon}{k_n} \right)^{\frac{p}{3}} \left( \frac{k_0}{k_n} \right)^{\delta \zeta_p}, \quad (8)$$

where  $C_p$  are dimensionless constants. We define the anomalous exponents as  $\zeta_p = \frac{p}{3} + \delta \zeta_p$ . The equivalent of Kolmogorov K41 theory yields for the shell models  $\zeta_p = \frac{p}{3}$ , and thus  $\delta \zeta_p$  is the deviation from Kolmogorov scaling. The equivalent of the exact 4/5th law [3] also holds in these models, and one can show that the third order structure function is given exactly by

$$S_3(k_n) = \frac{1}{2k_n(a-c)} \left( -\varepsilon + \left( \frac{a}{c} \right)^n \delta \right), \quad (9)$$

where  $\varepsilon$  is the mean energy dissipation rate and  $\delta$  is the mean helicity dissipation rate [15]. One can tune the large scale forcing in order to cancel this last contribution, or alternatively one can decrease its impact by choosing  $|\frac{a}{c}| < 1$  [15]. Apart from  $\zeta_3 = 1$  which is fixed by (9), the other exponents are anomalous, *i.e.*  $\zeta_p \neq \frac{p}{3}$ . While the K41 dimensional analysis and Eq. (9) hold for any values of the parameters (provided  $a + b + c = 0$ ), the values of the anomalous exponents depend on the choice of parameters  $c$  and  $\lambda$  [7]. They are quantitatively very close to the ones observed in fluid turbulence for the specific choice  $c = -0.5$  and  $\lambda = 2$  [15]. All our computations are carried out using this choice of parameters, unless stated otherwise.

For fixed parameters, the behaviour in the inertial range is universal. In this system, [this](#) means that it does not depend on the viscosity  $\nu$  and on the precise form of the forcing  $f_n$  as long as it only acts on large scales. While one usually introduces a deterministic forcing on the first two shells tuned to eliminate the spurious helicity flux, we rather consider, as common in field theoretical approaches of turbulence, a stochastic forcing, which can be chosen as Gaussian without loss of generality [40]. Its covariance is defined as

$$\langle f_n(t) f_{n'}(t') \rangle = 2N_{L-1,n} \delta(t-t') \delta_{nn'}, \quad (10)$$

where  $N_{L-1,n}$  is concentrated at the integral scale, *i.e.* it is non-zero for shells with  $k_n \simeq L^{-1}$ . In practice, we use the profile

$$N_{L-1,n} = D h(Lk_n), \quad h(x) = x^2 e^{-x^2}, \quad (11)$$

where  $D$  is the forcing amplitude.

## 2.2 Path integral formalism

The Sabra shell model (2) in the presence of the stochastic forcing (10) takes the form of a set of coupled Langevin equations. These stochastic equations can be cast into a path integral formalism using the Martin-Siggia-Rose-Janssen-de Dominicis procedure [45–47], which was implemented in the context of shell models in Ref. [40,48]. This procedure relies on the introduction of response fields  $\bar{v}_n$  and  $\bar{v}_n^*$  which play the role of Lagrange multipliers to enforce the equations of motion. Collecting the different fields in a multiplet  $V = (v, v^*, \bar{v}, \bar{v}^*)$  to alleviate notation, the generating functional associated with the dynamics of the shell model is given by

$$\mathcal{Z}[J] = \int \mathcal{D}[V] e^{-S[V] - \Delta \mathcal{S}_{L-1}[V] + \sum_{n,\alpha} \int_t V_{\alpha,n} J_{\alpha,n}}, \quad (12)$$

where we introduced the source multiplet  $J = (j, j^*, \bar{j}, \bar{j}^*)$ , and Greek indices  $\alpha = \{1, 2, 3, 4\}$  span the fields in the multiplet, whereas  $n \in \mathbb{Z}$  refers to the shell index. The action for the Sabra shell model, splitted in two parts for latter purpose, writes

$$S[V] = \sum_n \int_t \bar{v}_n^* (\partial_t v_n + \nu k_n^2 v_n - B_n[v, v^*]) + \text{c.c.}, \quad \Delta \mathcal{S}_{L-1}[V] = - \sum_n \int_t N_{L-1}(k_n) \bar{v}_n v_n^*, \quad (13)$$

where c.c. denotes the complex conjugate. This action is general for shell models, which differ only in the precise form of the non-linear interaction  $B[v, v^*]$ . We also consider the generating functional  $\mathcal{W} = \ln \mathcal{Z}$ . In the framework of equilibrium statistical mechanics, the functional  $\mathcal{Z}$  is the partition function of the system, and  $\mathcal{W}$  its free energy. In probability theory,  $\mathcal{Z}$  is analogous to the characteristic function, *i.e.* the generating function of moments, while  $\mathcal{W}$  is the generating

function of cumulants. They are simply promoted to functionals in the context of field theory since the random variables are here fluctuating spacetime-dependent fields. The central interest of these functionals is that all the statistical properties of the system can be derived from them. In particular the  $m$ -point correlation functions (generalisation of moments), or  $m$ -point connected correlation functions (generalisation of cumulants), can be computed by taking  $m$  functional derivatives of  $\mathcal{Z}$ , respectively  $\mathcal{W}$ , and evaluating them at zero values of the response fields.

The presence of forcing and dissipation ensures that the system reaches a non-equilibrium statistically stationary state. In the following, we thus assume that the statistics are invariant under time translations, and we introduce the Fourier transform of the fields in time. We use the following conventions:

$$\begin{aligned} f(\omega) &\equiv \mathcal{F}[f(t)] = \int_t e^{i\omega t} f(t) \\ f(t) &\equiv \mathcal{F}^{-1}[f(\omega)] = \int_{\omega} e^{-i\omega t} f(\omega) = \int_{\mathbb{R}} \frac{d\omega}{2\pi} e^{-i\omega t} f(\omega). \end{aligned} \quad (14)$$

The Sabra field theory can be studied by means of RG techniques, which we introduce in the following section.

### 3 Functional renormalisation group formalism

The functional renormalisation group is a modern formulation of the Wilsonian renormalisation group, which allows for functional and non-perturbative approximations [27–30]. The general idea underlying the renormalisation group is to perform a progressive averaging of the fluctuations of a system, may they be thermal, quantum or stochastic, in order to build the effective theory of the system at the macroscopic scale. It is endowed through FRG with a very versatile framework, which is used in a wide range of applications, both in high-energy physics (quantum gravity and QCD), condensed matter, quantum many-body systems and statistical mechanics, including disordered and non-equilibrium problems (for reviews see [27–30]).

In the context of turbulence, the FRG was employed to study homogeneous and isotropic turbulence in several works [31–33, 35, 36, 38, 49, 50]. As mentioned in the introduction, the main achievements so far are twofold: to show the existence of the fixed-point describing the universal properties of turbulence forced at large scales; to provide the expression of the spatio-temporal multi-point multi-time Eulerian correlations, which is exact in the limit of large-wave-numbers [34]. In this work, we resort to the FRG method to study shell models of turbulence.

#### 3.1 General framework for shell models

The goal of the FRG is to achieve the integration of the fluctuations in the path integral (12) progressively. For this, one introduces a continuous wave-number scale parameter  $\kappa$ , and a cut-off term which suppresses all fluctuation modes on shells  $k_n$  below the RG scale  $\kappa$ . This cut-off term, also called regulator, usually takes the form of an additional quadratic term  $\Delta\mathcal{S}_{\kappa}$  (analogous to a mass) in the path integral action, which reads for the shell model

$$\Delta\mathcal{S}_{\kappa}[V] = \frac{1}{2} \sum_n \int_t V_{\alpha,n} \mathcal{R}_{\kappa,n}^{\alpha\beta} V_{\beta,n}. \quad (15)$$



The cut-off functions  $\mathcal{R}_{\kappa,n}^{\alpha\beta}$  are required to be very large for modes with  $k_n \lesssim \kappa$  such that those modes contribution in the path integral is suppressed, and to vanish for modes with  $k_n \gtrsim \kappa$  such that those modes contribution is unaltered. Thus, at a given RG scale  $\kappa$ , only the fluctuations on shells  $n \gtrsim \ln(\kappa)/\ln(\lambda)$  are integrated in the path integral, and as  $\kappa \rightarrow 0$ , all fluctuations are progressively included. Note that we restrict to memoryless cutoff functions, that is cutoff functions which are white in time. This choice simplifies the calculations and was shown to yield reliable results in many applications of FRG to non-equilibrium systems [30].

We conform to a common choice in turbulence applications [31, 33] and equate the inverse integral scale and the RG scale  $\kappa$  ( $\kappa = L^{-1}$ ). The integral scale forcing term thus becomes a component of the regulator  $\mathcal{R}_{\kappa,n}^{\bar{v}\bar{v}^*} = -\frac{1}{2}N_{\kappa,n}$ , and gives a nice physical interpretation of the RG flow: turbulence gradually builds up as  $L$  grows, and developed turbulence is obtained as  $L \rightarrow \infty$  which corresponds to a fixed point of the RG procedure. We also include in the regulator the term:

$$\mathcal{R}_{\kappa,n}^{v\bar{v}^*} = R_{\kappa,n}, \quad R_{\kappa,n} = \nu k_n^2 r\left(\frac{k_n}{\kappa}\right), \quad (16)$$

which can be interpreted as a scale-dependent damping friction term at scale  $\kappa$  [33]. We choose  $r$  as the usual Wetterich cut-off

$$r(x) = \frac{\alpha}{e^{x^2} - 1}, \quad (17)$$

where  $\alpha$  is a parameter introduced to perform a sensitivity (error) analysis in Appendix D. The complete regulator matrix, with the fields ordered as  $(v, v^*, \bar{v}, \bar{v}^*)$ , thus reads:

$$\mathcal{R}_{\kappa,n} = \begin{pmatrix} 0 & 0 & 0 & R_{\kappa,n} \\ 0 & 0 & R_{\kappa,n} & 0 \\ 0 & R_{\kappa,n} & 0 & -N_{\kappa,n} \\ R_{\kappa,n} & 0 & -N_{\kappa,n} & 0 \end{pmatrix}, \quad (18)$$

which is the most general form since the  $\nu v^*$  sector vanishes for causality reasons [51], while any contribution involving two conjugated field or two non-conjugated fields is incompatible with translational invariance.

The addition of  $\Delta\mathcal{S}_\kappa$  turns  $\mathcal{Z}$  into a scale-dependent generating functional:

$$\mathcal{Z}_\kappa[J] = \int \mathcal{D}[V] e^{-\mathcal{S}[V] - \Delta\mathcal{S}_\kappa[V] + \sum_{n,\alpha} \int_t V_{\alpha,n} J_{\alpha,n}}. \quad (19)$$

In the functional renormalisation group formalism, the central object is the effective average action  $\Gamma_\kappa$ , defined as the Legendre transform of  $\mathcal{W}_\kappa = \ln \mathcal{Z}_\kappa$ :

$$\Gamma_\kappa[U] = \left[ \sum_{n,\alpha} \int_t U_{\alpha,n} J_{\alpha,n} \right] - \mathcal{W}_\kappa[J] - \Delta\mathcal{S}_\kappa[U], \quad (20)$$

where the value of  $J$  is fixed by the relation

$$U \equiv \langle V \rangle = \frac{\delta \mathcal{W}_\kappa[J]}{\delta J}, \quad (21)$$

such that  $U$  corresponds to the expectation value of  $V$ . The functional  $\Gamma_\kappa$  turns out to be well-suited to implement functional and non-perturbative approximation schemes [27, 30]. It is solution of the exact Wetterich equation:

$$\partial_\kappa \Gamma_\kappa = \frac{1}{2} \text{Tr} \sum_{n,n'} \int_t \partial_\kappa \mathcal{R}_{\kappa,nn'}(t) \cdot G_{\kappa,n'n}(t), \quad G_{\kappa,n} = \left[ \Gamma_{\kappa,n}^{(2)} + \mathcal{R}_{\kappa,n} \right]^{-1}, \quad (22)$$



where  $\Gamma_\kappa^{(2)}$  is the Hessian of the effective average action. This flow equation allows one to continuously interpolate between the microscopic theory at some UV scale  $\Lambda$ , which is here the shell model, *i.e.*  $\Gamma_{\kappa=\Lambda}[U] = \mathcal{S}[U]$  defined by (13), and the effective theory as  $\kappa \rightarrow 0$ , *i.e.*  $\Gamma_{\kappa=0} \equiv \Gamma$ . The functional  $\Gamma$  is called in field theory the generating functional of one-particle irreducible correlation functions. It corresponds in the context of equilibrium statistical mechanics to the Gibbs free energy. In non-equilibrium systems, it still incorporates the effects of fluctuations at all scales, and allows one to compute all the statistical properties of the system. Since the functionals  $\Gamma_\kappa$  and  $\mathcal{W}_\kappa$  are related by a Legendre transform (20), the knowledge of the set of  $\Gamma_\kappa^{(m)}$  is equivalent to the knowledge of the set of  $\mathcal{W}_\kappa^{(m)}$ . In particular, the structure functions can be computed from the propagator  $G_\kappa$  and the vertices  $\Gamma_\kappa^{(m)}$ , see Sec. 4.3. The flow equation for the  $\Gamma_\kappa^{(m)}$  can be obtained by taking  $m$  functional derivatives of (22) with respect to the fields. For instance, this yields for the flow equation of the two-point function  $\Gamma_\kappa^{(2)}$  the following flow equation

$$\begin{aligned} \partial_\kappa \tilde{\Gamma}_{\kappa,nn'}^{U_\alpha U_{\alpha'}}(\omega) = & \text{Tr} \sum_{m_i} \int_{\omega_1} \partial_\kappa \tilde{\mathcal{R}}_{\kappa,m_1 m_2}(\omega_1) \cdot \tilde{G}_{\kappa,m_2 m_3}(\omega_1) \cdot \left[ \frac{1}{2} \tilde{\Gamma}_{\kappa,nn'm_3 m_4}^{U_\alpha U_{\alpha'},(2)}(\omega, -\omega, \omega_1) \cdot \tilde{G}_{\kappa,m_4 m_1}(\omega_1) \right. \\ & \left. - \tilde{\Gamma}_{\kappa,nn'm_3 m_4}^{U_\alpha,(2)}(\omega, \omega_1) \cdot \tilde{G}_{\kappa,m_4 m_5}(\omega + \omega_1) \cdot \tilde{\Gamma}_{\kappa,n'm_5 m_6}^{U_{\alpha'},(2)}(-\omega, \omega + \omega_1) \cdot \tilde{G}_{\kappa,m_6 m_1}(\omega_1) \right], \end{aligned} \quad (23)$$

where the tilded quantities are defined as

$$\Gamma_{\kappa,m_1 \dots m_n}^{(n)}(\omega_1, \dots, \omega_n) = 2\pi \delta(\omega_1 + \dots + \omega_n) \tilde{\Gamma}_{\kappa,m_1 \dots m_n}^{(n)}(\omega_1, \dots, \omega_{n-1}). \quad (24)$$

They depend on one less frequency than their non-tilded counterpart owing to frequency conservation. We are thus explicitly focusing on the stationary state. The vertices  $\tilde{\Gamma}_\kappa^{(3)}$  and  $\tilde{\Gamma}_\kappa^{(4)}$  are here put in the form of  $4 \times 4$  matrices with one, *e.g.*  $\tilde{\Gamma}_\kappa^{U_{\alpha'},(2)}$ , respectively two, *e.g.*  $\tilde{\Gamma}_\kappa^{U_\alpha U_{\alpha'},(2)}$ , entries fixed to the external fields  $U_\alpha$  and  $U_{\alpha'}$  and external indices  $n$  and  $n'$ . The dot thus represents a matrix product in this notation. This flow equation can also be represented using Feynman diagrams as:

$$\partial_\kappa \tilde{\Gamma}_{\kappa,nn'}^{U_\alpha U_{\alpha'}} = \begin{array}{c} \text{---} \circlearrowleft \text{---} \\ \text{---} \text{---} \end{array} - \frac{1}{2} \begin{array}{c} \text{---} \circlearrowleft \text{---} \\ \text{---} \text{---} \end{array}, \quad (25)$$

where the vertices are given by the  $\Gamma_\kappa^{(m)}$ , the lines correspond to the propagator  $G_\kappa$ , and the cross stands for the regulator  $\mathcal{R}_\kappa$ . Since the propagator enters in all the flow equations, we first determine its general form.

### 3.2 General form of the propagator

The propagator  $G_\kappa$  is defined as the inverse of the Hessian of  $\Gamma_\kappa + \Delta\mathcal{S}_\kappa$ . From general considerations of causality, and translational invariance in space, there are only two independent terms in the Hessian of the effective average action, as for the regulator in (18). Using translational invariance in time, they take the following form in Fourier space

$$\begin{aligned} \mathcal{F} \left[ \frac{\delta^2 \Gamma_\kappa}{\delta \bar{u}_n(t) \bar{u}_{n'}^*(t')} \right] (\omega, \omega') &= \bar{\gamma}_{\kappa,n}(\omega) \delta_{nn'} 2\pi \delta(\omega + \omega') \\ \mathcal{F} \left[ \frac{\delta^2 \Gamma_\kappa}{\delta u_n(t) \bar{u}_{n'}^*(t')} \right] (\omega, \omega') &= \gamma_{\kappa,n}(\omega) \delta_{nn'} 2\pi \delta(\omega + \omega'), \end{aligned} \quad (26)$$

where  $\mathcal{F}$  denotes the Fourier transform defined in (14). Thus, the Hessian of  $\Gamma_\kappa$  is given by

$$\tilde{\Gamma}_{\kappa,nn'}^{(2)}(\omega) = \delta_{nn'} \begin{pmatrix} 0 & 0 & 0 & \gamma_{\kappa,n}(\omega) \\ 0 & 0 & \gamma_{\kappa,n}(\omega) & 0 \\ 0 & \gamma_{\kappa,n}(-\omega) & 0 & \bar{\gamma}_{\kappa,n}(\omega) \\ \gamma_{\kappa,n}(-\omega) & 0 & \bar{\gamma}_{\kappa,n}(-\omega) & 0 \end{pmatrix}. \quad (27)$$

Then, as  $\Gamma_\kappa^{(2)} + \tilde{\mathcal{R}}_\kappa$  is diagonal in shell index, its inverse is simply a matrix inverse, given by

$$\tilde{G}_{\kappa,nn'}(\omega) = \delta_{nn'} \begin{pmatrix} 0 & \bar{g}_{\kappa,n}(\omega) & 0 & g_{\kappa,n}(\omega) \\ \bar{g}_{\kappa,n}(-\omega) & 0 & g_{\kappa,n}(\omega) & 0 \\ 0 & g_{\kappa,n}(-\omega) & 0 & 0 \\ g_{\kappa,n}(-\omega) & 0 & 0 & 0 \end{pmatrix}. \quad (28)$$

with

$$g_{\kappa,n}(\omega) = \frac{1}{\gamma_{\kappa,n}(-\omega) + R_{\kappa,n}}, \quad \bar{g}_{\kappa,n}(\omega) = \frac{N_{\kappa,n} - \bar{\gamma}_{\kappa,n}(-\omega)}{|\gamma_{\kappa,n}(\omega) + R_{\kappa,n}|^2}. \quad (29)$$

### 3.3 Approximation schemes in FRG

The flow equation (22) is exact, but it is a functional non-linear partial differential equation which obviously cannot be solved exactly. In particular, as usual with non-linear equations, it is not closed, *i.e.* the flow equation for a given  $\Gamma_\kappa^{(m)}$  depends on higher-order vertex functions  $\Gamma_\kappa^{(m+1)}$  and  $\Gamma_\kappa^{(m+2)}$  (as manifest in (23)-(25) for  $m = 2$ ), such that it leads to an infinite hierarchy of flow equations. Thus one has to resort to some approximations. The key asset of the FRG formalism is that (22) lends itself to functional and non-perturbative approximation schemes. The most common one is called the derivative expansion as it consists in expanding  $\Gamma_\kappa$  in powers of spatial and temporal derivatives, while retaining the functional dependence in the fields. However, in the context of turbulence, we expect a rich behaviour at small scales, *i.e.* large wave-numbers, which is not *a priori* accessible through such a scheme. The alternative common approximation scheme rather consists in a vertex expansion, *i.e.* an expansion in powers of the fields, while retaining a functional dependence in the derivatives, or equivalently in wave-numbers and frequencies [27, 30].

In fact, for Navier-Stokes turbulence, it was shown that, owing to the general properties of the regulator and the existence of extended symmetries of the Navier-Stokes field theory, the flow equation for any  $\Gamma_\kappa^{(m)}$  can be closed (*i.e.* it does not depend any longer on higher-order  $\ell > m$  vertices) for large wave-numbers without further approximation than taking the large wave-number limit [34, 35]. Its solution at the fixed-point yields the exact general expression at leading order in large wave-number for the spatio-temporal dependence of arbitrary  $m$ -point Eulerian correlation functions. This expression gives the rigorous form of effects associated with random sweeping. However, this leading order term vanishes for equal times. It means that it does not encompass equal-time correlation functions, in particular structure functions. The random sweeping effect thus hides the intermittency corrections, in the sense that the latter are contained in sub-leading terms compared to sweeping.

In shell models, the effect of sweeping is concentrated in the zero mode (see Appendix A), and because of the locality of the interactions in shell indices, it does not affect the other modes. Hence, the intermittency effects are *a priori* more directly accessible, in the sense that they are not contained in subleading terms compared to the sweeping because the latter is absent. The

purpose of this work is to assess this hypothesis and access intermittency effects in these simplified models. Thus, we focus in the following on equal-time quantities, namely the structure functions, and compute them at the leading order of the vertex expansion. This indeed allows us to obtain anomalous exponents.

## 4 Fixed point and anomalous exponents

### 4.1 Leading order approximation

The leading order (LO) of the vertex expansion scheme consists in keeping the full functional dependence in wave-numbers of the two-point functions, while approximating higher-order vertices. At lowest order, we simply keep the vertices present in the microscopic action (13) and neglect the other ones. The corresponding Ansatz for the effective average action thus reads:

$$\Gamma_{\kappa}^{\text{LO}}[U] = \sum_n \int_t \left\{ \bar{u}_n^* [f_{\kappa,n}^{\lambda} \partial_t u_n + B_n[u, u^*] + f_{\kappa,n}^{\nu} u_n] - \frac{1}{2} \bar{u}^* f_{\kappa,n}^D \bar{u}_n + \text{c.c.} \right\}. \quad (30)$$

It essentially bares the same form as the microscopic action (13), but with renormalised, or effective, parameters,  $f_{\kappa,n}^{\nu}$ ,  $f_{\kappa,n}^D$ , and  $f_{\kappa,n}^{\lambda}$ , which can acquire a wave-number (shell index) dependence along the flow (hence the name functional RG). On the other hand, the interactions contained in  $B[u, u^*]$  are not renormalised, *i.e.* they keep their microscopic forms. This is of course a (rather crude) approximation, since all vertices compatible with the symmetries are generated in principle by the flow and should be included. Moreover, the frequency dependence of the three functions  $f_{\kappa,n}^{\nu}$ ,  $f_{\kappa,n}^D$ , and  $f_{\kappa,n}^{\lambda}$  is also neglected for simplicity. As shown in the following, the LO approximation is sufficient to describe the fixed-point and accurately compute the anomalous scaling of the second-order structure function. However, it does not allow for multi-scaling behaviour. Its limitations are further discussed in Sec. 4.3.

The task is now to compute the flow equations of the three functions  $f_{\kappa,n}^{\nu}$ ,  $f_{\kappa,n}^D$ , and  $f_{\kappa,n}^{\lambda}$ , and to solve them. The statistical properties of the model can be computed at the end of the flow, in the limit  $\kappa \rightarrow 0$ , once all the fluctuations have been averaged out. In particular, if the RG flow reaches a fixed point (which is expected from the observation of universality and scale invariance), the structure functions can be calculated from the fixed-point functions.

Taking two functional derivatives of (30) with respect to  $\bar{u}_n^*$ ,  $u_{n'}$ , and  $\bar{u}_{n'}^*$ ,  $\bar{u}_{n'}$ , and obtains

$$\gamma_{\kappa,n}(\omega) = i\omega f_{\kappa,n}^{\lambda} + f_{\kappa,n}^{\nu}, \quad \bar{\gamma}_{\kappa,n}(\omega) = -f_{\kappa,n}^D, \quad (31)$$

with  $\gamma_{\kappa}$  and  $\bar{\gamma}_{\kappa}$  defined in (26). The flow equations for the three functions can thus be obtained from the flow of the two-point functions  $\Gamma_{\kappa}^{u\bar{u}^*}$  and  $\Gamma_{\kappa}^{\bar{u}\bar{u}^*}$  as

$$\partial_{\kappa} f_{\kappa,n}^{\nu} = \Re e \left[ \partial_{\kappa} \tilde{\Gamma}_{\kappa,nn}^{u\bar{u}^*} \right] \quad \partial_{\kappa} f_{\kappa,n}^{\lambda} = \frac{1}{i\omega} \Im m \left[ \partial_{\kappa} \tilde{\Gamma}_{\kappa,nn}^{u\bar{u}^*} \right] \quad \partial_{\kappa} f_{\kappa,n}^D = -\partial_{\kappa} \tilde{\Gamma}_{\kappa,nn}^{\bar{u}\bar{u}^*}. \quad (32)$$

The exact flow equations for  $\Gamma_{\kappa}^{u\bar{u}^*}$  and  $\Gamma_{\kappa}^{\bar{u}\bar{u}^*}$  are given by (23). Within the LO approximation, all 4-point vertices vanish, and there remain only two types of 3-point vertices (and their complex

conjugate), which originate from the  $B[u, u^*]$  term in (30):

$$\begin{aligned}
 \gamma_{\kappa, n_1 n_2 n_3}^{uu\bar{u}^*}(\omega_1, \omega_2, \omega_3) &\equiv \mathcal{F} \left[ \frac{\delta^{(3)} \Gamma_{\kappa}}{\delta u_{n_1}(t_1) \delta u_{n_2}(t_2) \delta \bar{u}_{n_3}^*(t_3)} \right] \\
 &= -ick_{n_3-1} (\delta_{n_3 n_1+1} \delta_{n_3 n_2+2} + \delta_{n_3 n_1+2} \delta_{n_3 n_2+1}) 2\pi \delta(\omega_1 + \omega_2 + \omega_3) \\
 \gamma_{\kappa, n_1 n_2 n_3}^{u\bar{u}^*}(\omega_1, \omega_2, \omega_3) &\equiv \mathcal{F} \left[ \frac{\delta^{(3)} \Gamma_{\kappa}}{\delta u_{n_1}(t_1) \delta u_{n_2}^*(t_2) \delta \bar{u}_{n_3}^*(t_3)} \right] \\
 &= i (ak_{n_2} \delta_{n_1 n_2+1} \delta_{n_1 n_3+2} + bk_{n_3} \delta_{n_1 n_2+2} \delta_{n_1 n_3+1}) 2\pi \delta(\omega_1 + \omega_2 + \omega_3). \quad (33)
 \end{aligned}$$

Inserting into the flow equation (23) the explicit expressions at LO for the propagator  $G_{\kappa}$  given by (28), (29) and (31) and the vertices  $\Gamma_{\kappa}^{(3)}$  given by (33), one obtains the flow equation for the two-point functions  $\Gamma_{\kappa}^{uu^*}$  and  $\Gamma_{\kappa}^{\bar{u}\bar{u}^*}$ , from which the flows of  $f_{\kappa, n}^v$ ,  $f_{\kappa, n}^D$ , and  $f_{\kappa, n}^{\lambda}$  can be deduced following (32). The expression of these flow equations is given in Appendix B.

## 4.2 Fixed-point solution

The flow equations for the three sets  $(f_{\kappa}^v)_{n \in \mathbb{Z}}$ ,  $(f_{\kappa}^D)_{n \in \mathbb{Z}}$  and  $(f_{\kappa}^{\lambda})_{n \in \mathbb{Z}}$  (given in Appendix B by (62), (63) and (64) respectively) form a set of coupled ordinary differential equations. The simplification of shell models compared to the full hydrodynamic equations thus also occurs for the RG equations, which are originally partial differential equations. Moreover, the usual integral over the loop wave-vector is transformed into a discrete sum over shell indices. Owing to the locality of the interaction term  $B[u, u^*]$ , only neighbouring shells are coupled, such that this sum is strongly localised around the external shell  $n$  (the shell for which the flow is considered). This ensures that the flow at a given shell  $n$  strictly stops when  $k_n \gtrsim \kappa$ , and the functions for  $m > n$  do not evolve any more for the rest of the flow. Thus, a fixed-point gradually builds up as the RG scale is lowered. Contrarily to the usual case, one needs not non-dimensionalise all quantities with the RG scale to evidence the fixed-point. The integration of the flow can be carried out directly for the dimensionful quantities. The initial condition of the flow corresponds to the microscopic action (13), that is

$$f_{\kappa=\Lambda, n}^v = \nu k_n^2, \quad f_{\kappa=\Lambda, n}^{\lambda} = 1, \quad f_{\kappa=\Lambda, n}^D = 0. \quad (34)$$

Note that the initial condition for  $f_{\kappa}^D$  is zero because the forcing has been incorporated in the regulator part.

The numerical procedure to integrate the flow equations is detailed in Appendix C. The chosen parameters are  $\lambda = 2$  (shell ratio),  $c = -1/2$  (shell model parameter),  $N = 80$  (total number of shells),  $\varepsilon = \sum_n N_n = 7.2 \times 10^{-6}$  (mean energy injection rate),  $\eta^{-1} = (\varepsilon/\nu^3)^{1/4} = 291$  (inverse Kolmogorov scale),  $\Lambda = 2^4 \times k_N$  (microscopic scale),  $\alpha = 1$  (cut-off parameter). The result is displayed in Fig. 1. One observes that the functions indeed gradually deform from the large shell indices towards the small ones as the RG scale is decreased. Thus a stable attractive fixed point of the renormalisation flow is attained, as anticipated. The fixed-point functions, denoted  $f_{0, n}^v$ ,  $f_{0, n}^D$ ,  $f_{0, n}^{\lambda}$ , exhibit power-law behaviours in the inertial range,

$$f_{0, n}^v \sim k_n^{\eta_v}, \quad f_{0, n}^{\lambda} \sim k_n^{\eta_{\lambda}}, \quad f_{0, n}^D \sim k_n^{\eta_D}, \quad (35)$$

with scaling exponents  $\eta_v = 0.633 \pm 0.004$ ,  $\eta_{\lambda} = 0.102 \pm 0.005$  and  $\eta_D = -0.007 \pm 0.018$ . These exponents are anomalous, since one expects from dimensional analysis  $\eta_v = 2/3$  and  $\eta_D = \eta_{\lambda} = 0$ . This leads to anomalous scaling for the structure functions, which we study in Sec. 4.3. The error

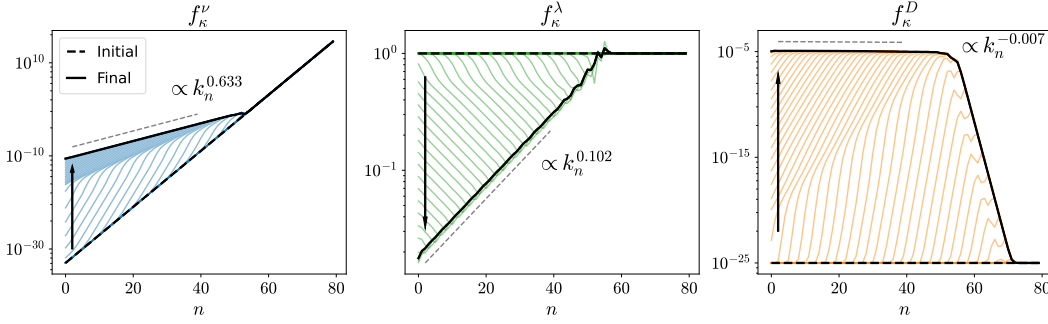


Figure 1: Evolution of the three functions  $f_{\kappa,n}^\nu$ ,  $f_{\kappa,n}^D$ , and  $f_{\kappa,n}^\lambda$  along the RG flow, *i.e.* as the RG scale  $\kappa$  is decreased, as indicated by the arrows. At the microscopic scale  $\kappa = \Lambda$ , the three functions are given by the initial condition (34) represented by the thick dashed lines. The fixed point, represented by thick solid lines, gradually builds up along the flow until all fluctuation modes have been averaged out when  $\kappa \rightarrow 0$ , *i.e.*  $\kappa$  tends to the  $n = 0$  shell.

bars indicated here and in the remainder of the paper are errors from the fit. They are computed as one standard deviation of the fit, and the fit range is chosen to minimise this error. This numerical error is larger than the error related to the choice of the cutoff, which is reported in Appendix D. We note that this error does not account for the choice of the LO approximation itself.

### 4.3 Structure functions

The fixed-point provides the limit  $\kappa \rightarrow 0$  of the RG flow which describes the universal statistical properties of the model, resulting from the integration of all the fluctuations. Within the LO approximation, all the structure functions are expressed in terms of the three fixed-point functions  $f_{0,n}^\nu$ ,  $f_{0,n}^D$ ,  $f_{0,n}^\lambda$ , and the bare vertices (33).

#### 4.3.1 Second order structure function

The second order structure function  $S_2(k_n)$  is given by

$$S_2(k_n) = \langle v_n(t)v_n^*(t) \rangle = \int_{\omega} \frac{\delta^2 \mathcal{W}_{\kappa}}{\delta j_n \delta j_n^*} \Big|_{\kappa \rightarrow 0} = \int_{\omega} \bar{g}_{\kappa,n}(\omega) \Big|_{\kappa \rightarrow 0} = \frac{f_{0,n}^D}{2f_{0,n}^\nu f_{0,n}^\lambda}, \quad (36)$$

where the integration over  $\omega$  can be carried out analytically within the LO approximation owing to the simple form of  $\bar{g}_{\kappa,n}$  given by (29), (31). The result is shown in Fig. 2. As expected from (36),  $S_2$  follows a power-law in the inertial range  $S_2 \sim k_n^{-\zeta_2}$  with  $\zeta_2 = \eta_\nu + \eta_\lambda - \eta_D$ . It yields  $\zeta_2 = 0.741 \pm 0.017$ , which is anomalous, since it deviates from the K41 prediction  $\zeta_2 = 2/3$ . Hence the FRG allows one to capture the intermittency exponent for  $S_2$ . The value for  $\zeta_2$  obtained is in good agreement with the value from numerical simulations  $\zeta_2 \simeq 0.720 \pm 0.008$  [15]. The constant  $C_2$  can be estimated from  $(k_n/\epsilon)^{\zeta_2} S_2$ , as shown in the inset of Fig. 2. One obtains  $C_2 \simeq 1.15$ . We did not find an estimate of this constant in numerical simulations to compare with.

We have checked that  $\zeta_2$  is universal, in the sense that its value does not change when varying the microscopic parameters  $\nu$  and  $D$  associated with the dissipation and forcing. We observed that varying  $\nu$  simply results in a change of the Kolmogorov scale  $\eta$ , and thus amounts to shifting the

lower boundary of the inertial range. Varying the forcing amplitude  $D$  induces a change in the mean injection rate  $\varepsilon$ . Thus, it simply changes the normalisation of  $S_2$ , *i.e.* it results in a global shift of  $S_2$  in logscale.

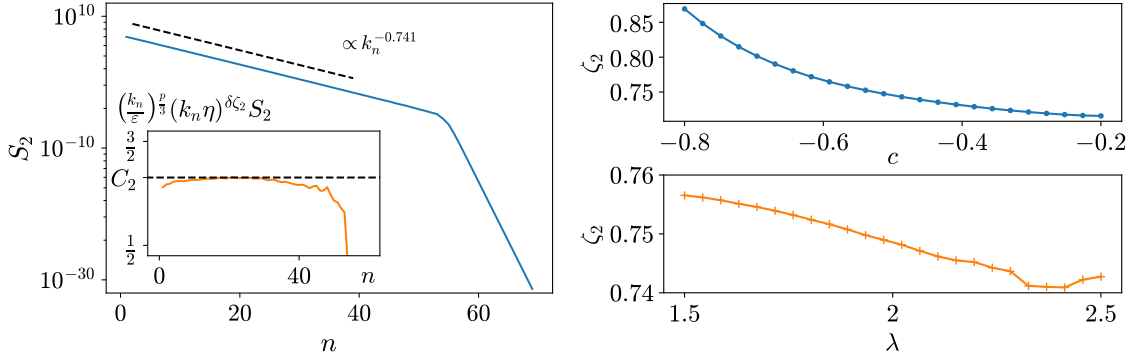


Figure 2: *Left panel:* Second order structure function  $S_2$  from FRG at LO approximation as a function of the shell index  $n$ , with the  $C_2$  constant shown in inset, for  $c = -1/2$  and  $\lambda = 2$ . *Right panel:* Anomalous exponent  $\zeta_2$  of the second-order structure function  $S_2$  as a function of the  $c$  parameter of the Sabra model (*top panel*) and of the shell ratio  $\lambda$  (*bottom panel*).

On the other hand, the value of  $\zeta_2$  depends on the choice of the parameters of the Sabra model, namely the  $c$  parameter of the non-linear interaction (2), and the shell ratio  $\lambda$ . The result for  $S_2$  presented in the left panel of Fig. 2 is obtained for the standard choice  $c = -1/2$  and  $\lambda = 2$ . We have also computed the variations of  $\zeta_2$  when varying the parameters  $c$  and  $\lambda$ , which are displayed in the right panel of Fig. 2. The exponent is anomalous in all the range of  $c$  and  $\lambda$  probed, and smoothly depends on these parameters. To the best of our knowledge, there is no other quantitative estimate of  $\zeta_2$  from numerical simulations of the GOY or Sabra models for values of  $c$  and  $\lambda$  other than  $c = -1/2$  and  $\lambda = 2$ .

### 4.3.2 Third order structure function

Since the two generating functionals  $\mathcal{W}_\kappa$  and  $\Gamma_\kappa$  are related by a Legendre transform (20), one has the following chain-rule relation

$$\frac{\delta \mathcal{W}_\kappa}{\delta J_{\alpha,n}(t)} = - \int_{t'} \sum_{n',\alpha'} \frac{\delta U_{\alpha',n'}(t')}{\delta J_{\alpha,n}(t)} \frac{\delta \Gamma_\kappa}{\delta U_{\alpha',n'}(t')} = - \int_{t'} \sum_{n'} G_{\kappa,nn'}^{U_\alpha U_{\alpha'}}(t,t') \Gamma_{\kappa,n'}^{U_{\alpha'}}(t'), \quad (37)$$

neglecting the linear term in (20) which plays no role for higher-order derivatives. Using this relation, one obtains for the third-order structure function

$$\begin{aligned} S_3(k_n) &= \Im \langle v_{n-1} v_n v_{n+1}^* \rangle = \Im \left[ \frac{\delta^3 \mathcal{W}}{\delta j_{n-1}(t) j_n(t) j_{n+1}^*(t)} \right] \\ &= - \Im \sum_{m_i} \sum_{\alpha,\beta,\gamma} \int_{\omega_1,\omega_2} \tilde{G}_{\kappa,n-1m_1}^{uU_\alpha}(\omega_1) \tilde{G}_{\kappa,nm_2}^{uU_\beta}(\omega_2) \tilde{\Gamma}_{\kappa,m_1m_2m_3}^{U_\alpha U_\beta U_\gamma}(\omega_1,\omega_2) \tilde{G}_{\kappa,n+1m_3}^{u^*U_\gamma}(-\omega_1-\omega_2). \end{aligned} \quad (38)$$

Within the LO approximation, the vertices  $\tilde{\Gamma}_\kappa^{(3)}$  are just the bare ones (33), since no renormalisation of the vertices is included in the LO Ansatz (30). Hence, the scaling exponent of  $S_3$  is completely fixed by the scaling behaviour of the three functions  $f_{\kappa,n}^\nu$ ,  $f_{\kappa,n}^D$  and  $f_{\kappa,n}^\lambda$ . Indeed, inserting the LO expressions for the propagator and vertices into (38), one obtains

$$S_3(k_n) = \frac{k_n \left( a \frac{\tilde{f}_{\kappa,n+1}^D \tilde{f}_{\kappa,n-1}^D}{\tilde{f}_{\kappa,n+1}^\nu \tilde{f}_{\kappa,n-1}^\nu} + b \frac{\tilde{f}_{\kappa,n+1}^D \tilde{f}_{\kappa,n}^D}{\tilde{f}_{\kappa,n+1}^\nu \tilde{f}_{\kappa,n}^\nu} + c \frac{\tilde{f}_{\kappa,n}^D \tilde{f}_{\kappa,n-1}^D}{\tilde{f}_{\kappa,n}^\nu \tilde{f}_{\kappa,n-1}^\nu} \right)}{4(\tilde{f}_{\kappa,n-1}^\nu f_{\kappa,n}^\lambda f_{\kappa,n+1}^\lambda + \tilde{f}_{\kappa,n}^\nu f_{\kappa,n-1}^\lambda f_{\kappa,n+1}^\lambda + \tilde{f}_{\kappa,n+1}^\nu f_{\kappa,n-1}^\lambda f_{\kappa,n}^\lambda)}. \quad (39)$$

In this expression, the frequency integrals have been performed analytically since the three running functions do not depend on frequencies. It is clear that  $S_3$  simply inherits from the anomalous exponents of  $f_0^\nu$ ,  $f_0^D$  and  $f_0^\lambda$  in the limit  $\kappa \rightarrow 0$ , yielding  $\zeta_3 = 3\eta_\nu + 2\eta_\lambda - 2\eta_D - 1$ . The result is shown in Fig. 3. One finds  $\zeta_3 = 1.113 \pm 0.039$ , which is a 10% deviation from the exact exponent  $\zeta_3 = 1$ . This can be interpreted as a measure of the error due to the LO Ansatz.

Alternatively, one can use the knowledge of  $S_2$  from the FRG calculation to determine  $S_3$  using the equation of motion. Indeed, let us follow [15] and multiply the equation of motion (2) by  $u_n^*$ , take the average, and assume stationarity. We then obtain

$$\nu k_n^2 S_2(k_n) = a k_{n+1} S_3(k_{n+1}) + b k_n S_3(k_n) + c k_{n-1} S_3(k_{n-1}) + N_n. \quad (40)$$

The last term was calculated within the path integral formalism as

$$\langle u_n^*(t) f_n(t) \rangle = \lim_{\delta t \rightarrow 0^+} \sum_{n'} G_{nn'}^{\bar{u}^* \bar{u}}(t + \delta t, t) N_{n'} = \lim_{\delta t \rightarrow 0^+} \int_{\omega} e^{-i\omega \delta t} G_{nn}^{\bar{u}^* \bar{u}}(\omega) N_n = N_n, \quad (41)$$

where the last equality results from Ito's discretisation. Knowing  $S_2$ , this constitutes a recursion relation for  $S_3$ . Hence, using the FRG result for  $S_2$  obtained at LO, one can construct  $S_3$  shell by shell starting from  $n = N$  where  $N$  denotes the maximum shell index. The values of  $S_2$  for the shell  $N + 1$  is approximated using the power-law extrapolation described in Appendix C. The resulting  $S_3$  is shown in Fig. 3. Interestingly, this method allows us to access the behaviour of  $S_3$  both in the inertial and dissipative range. In the inertial range, we recover the exact result  $\zeta_3 = 1$  (up to a numerical error below  $\sim 10^{-6}$ ). Moreover, the constant  $C_3$  in (8) can be evaluated by dividing  $S_3$  by  $\varepsilon/k_n$ , where  $\varepsilon$  is given by  $\varepsilon = \sum_n N_n$ . The result is shown in the inset of Fig. 3, and it coincides with the exact result  $C_3 = 1/(2(c - a)) = 1/3$  given by (9). This calculation hence also offers an independent check of the determination of  $\varepsilon$ .

### 4.3.3 Higher order structure functions

A general fourth order structure function is defined as

$$\left[ \frac{\delta^4 \mathcal{W}}{\delta J_{\alpha_1, n_1}(t) J_{\alpha_2, n_2}(t) J_{\alpha_3, n_3}(t) J_{\alpha_4, n_4}(t)} \right] =$$

$$- \sum_{m_i} \sum_{\beta_i} \int_{\omega_i} \tilde{G}_{\kappa, n_1 m_1}^{U_{\alpha_1} U_{\beta_1}}(\omega_1) \tilde{G}_{\kappa, n_2 m_2}^{U_{\alpha_2} U_{\beta_2}}(\omega_2) \tilde{G}_{\kappa, n_3 m_3}^{U_{\alpha_3} U_{\beta_3}}(\omega_3) \tilde{\Gamma}_{\kappa, m_1 m_2 m_3 m_4}^{U_{\beta_1} U_{\beta_2} U_{\beta_3} U_{\beta_4}}(\omega_1, \omega_2, \omega_3) \tilde{G}_{\kappa, n_4 m_4}^{U_{\alpha_4} U_{\beta_4}}(-\omega_1 - \omega_2 - \omega_3)$$

$$+ \sum_{m_i} \sum_{\beta_i} \int_{\omega_i} \tilde{G}_{\kappa, n_1 m_1}^{U_{\alpha_1} U_{\beta_1}}(\omega_1) \tilde{G}_{\kappa, n_2 m_2}^{U_{\alpha_2} U_{\beta_2}}(\omega_2) \tilde{\Gamma}_{\kappa, m_1 m_2 m_5}^{U_{\beta_1} U_{\beta_2} U_{\beta_5}}(\omega_1, \omega_2) \tilde{G}_{\kappa, m_5 m_6}^{U_{\beta_5} U_{\beta_6}}(\omega_1 + \omega_2)$$

$$\times \tilde{\Gamma}_{\kappa, m_6 m_3 m_4}^{U_{\beta_6} U_{\beta_3} U_{\beta_4}}(\omega_1 + \omega_2, \omega_3) \tilde{G}_{\kappa, n_3 m_3}^{U_{\alpha_3} U_{\beta_3}}(\omega_3) \tilde{G}_{\kappa, n_4 m_4}^{U_{\alpha_4} U_{\beta_4}}(-\omega_3 - \omega_1 - \omega_2) + \text{permutations}. \quad (42)$$



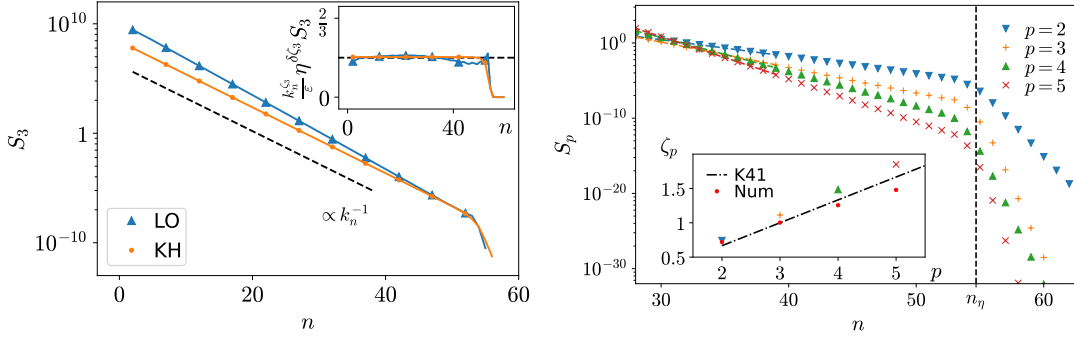


Figure 3: *Left panel*: Third order structure function from FRG computed using two methods. LO: direct reconstruction of  $S_3$  according to (39) within the LO Ansatz; KH: computation of  $S_3$  from the recursion relation (40) using the LO result for  $S_2$ . The corresponding  $C_3$  constants are shown in the inset. The exact exponent  $\zeta_3 = 1$  and constant  $C_3 = 1/(2(c - a)) = 1/3$  are recovered using the KH method. *Right panel*: Structure functions  $S_p(k_n)$  as a function of the shell index  $n$  for the orders  $p = 2$  to  $p = 5$ , from FRG within the LO approximation. The corresponding exponents  $\zeta_p$  as a function of the order  $p$  are shown in inset (symbols), and compared with K41 theory (black dashed line), and results from the numerical simulations of [15] (red dots).

Within the LO approximation, there is no 4-point vertex so the term in the first line vanishes, and the only three-point vertices contributing in the second line are the bare ones (33). Thus, one cannot construct a purely local structure function  $S_4(k_n)$  corresponding to  $n_1 = n_2 = n_3 = n_4$ . However, other “nearly local” configurations preserving translational invariance exist, they are listed in Appendix F. They are expected to display similar scaling properties. In fact, this has been verified in recent numerical simulations of the Sabra model [52].

Within the LO approximation, the following fourth-order structure function can be constructed and is non-zero

$$S_4(k_n) \equiv \langle v_n v_n^* v_{n+1} v_{n+1}^* \rangle = \frac{\delta^4 \mathcal{W}}{\delta j_n(t) j_n^*(t) j_{n+1}(t) j_{n+1}^*(t)}. \quad (43)$$

Its expression is given in Appendix E. The result is displayed in Fig. 3. It is clear from this expression that the anomalous scaling of  $S_4$  is inherited from the one of the three functions  $f_0^\nu$ ,  $f_0^D$  and  $f_0^\lambda$ . Indeed, one has  $\zeta_4 = 5\eta_\nu + 3\eta_\lambda - 3\eta_D - 2$ .

In fact, this analysis applies to all higher order structure functions within the LO approximation. At a given order  $p$ , the only structure function which is non-zero is constructed from  $p - 2$  bare vertices,  $p$  propagator  $G^{\bar{u}^*u}$  and  $p$  propagator  $G^{u^*u}$ . Thus, the scaling exponent of the  $p$ -th order structure function is completely fixed in terms of the three functions  $f_0^\nu$ ,  $f_0^D$  and  $f_0^\lambda$ , and is given by  $\zeta_p = \eta_\nu + \eta_\lambda - \eta_D + (2 - p)(1 + \eta_D - 2\eta_\nu - \eta_\lambda)$ , which is anomalous but affine in  $p$ . This scaling is thus uni-fractal, it is equivalent to that of a  $\beta$ -model [41].

This is clearly an artefact of the LO approximation, since the only non-trivial renormalisation taken into account in the LO Ansatz is that of the two-point functions. Hence, it allows one to capture the anomalous scaling of  $S_2$ , but it is not sufficient to access multi-fractal behaviour. For this, one should account for the renormalisation of higher-order vertices, at least 3-point and 4-point ones. This would allow for a contribution to the anomalous scaling independent of the one due to 2-point functions. An alternative promising route would be to account for a functional fre-

quency dependence in addition to the shell index dependence in the renormalisation of the 2-point functions  $f_{\kappa,n}^\nu$ ,  $f_{\kappa,n}^D$  and  $f_{\kappa,n}^\lambda$ . Indeed, we show in [52] that one can extract information about the intermittency exponent of a given order structure function from the time (or frequency) dependence of lower order correlation functions. These two routes to improve the LO approximation deserve further investigations.

## 5 Effect of long-range forcing

As mentioned in the introduction, the analogy between turbulence and critical phenomena (scale invariance, universality and anomalous scaling) sparked many RG studies of homogeneous isotropic turbulence [24–26]. The early implementations of the RG relied on a perturbative expansion in the renormalised coupling, which is controlled by the distance to an upper critical dimension  $\epsilon = d_c - d$ . However, for the Navier-Stokes equation, there is no upper critical dimension, and the interaction is the advection term, whose coupling is not adjustable (it is 1). The strategy to artificially introduce a small parameter has been to consider a forcing with a power law spectrum  $N(k) \propto k^{1-\epsilon}$  in  $d = 3$ . This forcing is hence long-range, *i.e.* it acts on all scales, whereas in physical situation turbulence is usually generated by a short-range forcing in scales, *i.e.* a forcing concentrated around the integral scale. The power-law forcing yields a kinetic energy spectrum  $E(k) \propto k^{1-2\epsilon/3}$ . Hence, hydrodynamic turbulence corresponds to  $\epsilon \rightarrow 4$ , for which the convergence of the perturbative expansion is questionable. Since in the framework of perturbative RG, the physical situation can only be accessed as this precarious limit from the long-range forcing, the question arises as to which extent it correctly describes hydrodynamic turbulence. In other words, are the multi-fractal behaviour of turbulence and the intermittency exponents universal with respect to *any* forcing, including a long-range one? This question was investigated using direct numerical simulations in [42–44], but it is difficult in numerics to disentangle the contributions of the long-range forcing from the large-scale (short-range) one and to resolve large crossovers in the power-laws. We show in the following that the long-range forcing and the short-range one correspond to two different universality classes.

### 5.1 Long-range forcing in the FRG framework

Our aim is to study the effect of a power law forcing on the statistical properties of the Sabra shell model. The forcing term in the model (2) is considered as a Gaussian random field with correlations encompassing both the usual short-range (SR) contribution (10) and a long-range (LR) one, such that the correlations of the forcing now take the form:

$$\langle f_n(t) f_{n'}(t') \rangle = 2(N_{L-1,n} + D^{\text{LR}} k_n^{-\rho}) \delta(t - t') \delta_{nn'}, \quad (44)$$

with  $D^{\text{LR}}$  the amplitude of the LR component and  $D$  the amplitude of the SR one defined in Eq. (11). Following the same procedure as in Sec. 2, this leads to an additional term in the action  $\mathcal{S}$  defined in (13) which reads

$$\mathcal{S}_{\text{LR}}[V] = - \int_t \sum_n D^{\text{LR}} k_n^{-\rho} \bar{u}_n \bar{u}_n^*, \quad (45)$$

Note that as this term does not have the properties expected for a regulator, we just leave it in the action. In essence, this simply means that the initial condition of the RG flow at the scale  $\kappa = \Lambda$

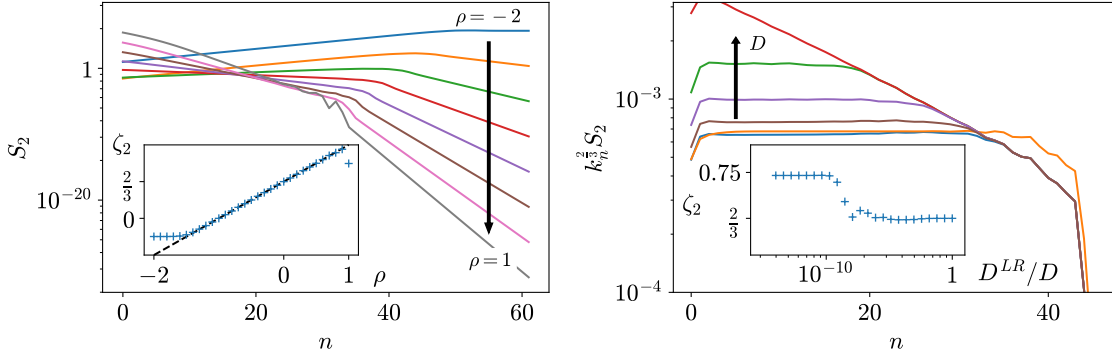


Figure 4: *Left panel:* Second order structure function  $S_2$  for a pure long-range (LR) forcing, *i.e.* without a large-scale component ( $D = 0$ ), termed short-range (SR). The inset shows the value of  $\zeta_2$  in the inertial range as a function of the LR exponent  $\rho$ . It takes the value  $\zeta_2^{\text{LR}} = \frac{2(1+\rho)}{3}$  (normal scaling) in the whole inertial range. *Right panel:* Compensated second order structure function in the presence of a SR component of the forcing with decreasing strength  $D \rightarrow 0$ , which evidences the crossover between the normal and the anomalous fixed points. The inset shows the corresponding value of  $\zeta_2$  as a function of  $D^{\text{LR}}/D$ .

is now changed to include the long-range forcing as

$$f_{\kappa=\Lambda, n}^D = D^{\text{LR}} k_n^{-\rho}. \quad (46)$$

The SR component is still incorporated in the  $\Delta S_{L-1}$  term.

In order to investigate the effect of the LR forcing, it is sufficient to work at the level of the LO approximation. The flow of the two-point functions  $\Gamma_{\kappa}^{(2)}$  can be computed in the exact same way as in Sec. 4 and the result is the same. However, since the initial condition of the flow is different, it leads to different solutions.

## 5.2 Purely long-range fixed-point

We first investigate the case where the forcing is purely long-range, that is the SR component is set to 0 by fixing  $D = 0$ . This means that the  $\mathcal{R}_{\kappa}^{\tilde{v}\tilde{v}^*} = -N_{\kappa, n}$  part of the regulator is removed. We solve the corresponding flow equations for the initial condition (46) with different values of  $\rho$  ranging from  $\rho = -2$  to  $\rho = 1$ . We observe that for each value of  $\rho$ , the flow reaches a fixed point as in the presence of the SR forcing. The corresponding second order structure functions are shown in Fig. 4. They all behave as a power law in the whole inertial range  $S_2 \sim k_n^{-\zeta_2^{\text{LR}}}$  with an exponent

$$\zeta_2^{\text{LR}} = \frac{2(1+\rho)}{3}, \quad (47)$$

as shown in the inset of Fig. 4. We attribute the saturation of  $\zeta_2^{\text{LR}}$  observed for  $\rho \lesssim -1.6$  to numerical effects, although we do not have a clear explanation for it. The exponent (47) corresponds to a normal (dimensional) scaling, with no anomalous corrections. Hence the purely LR fixed-point is non-intermittent (at the same LO level of approximation). Let us emphasise that it is also the case for  $\rho = 0$ , which corresponds to a constant (finite) forcing on all shells. For  $\rho \rightarrow 0$  (which is

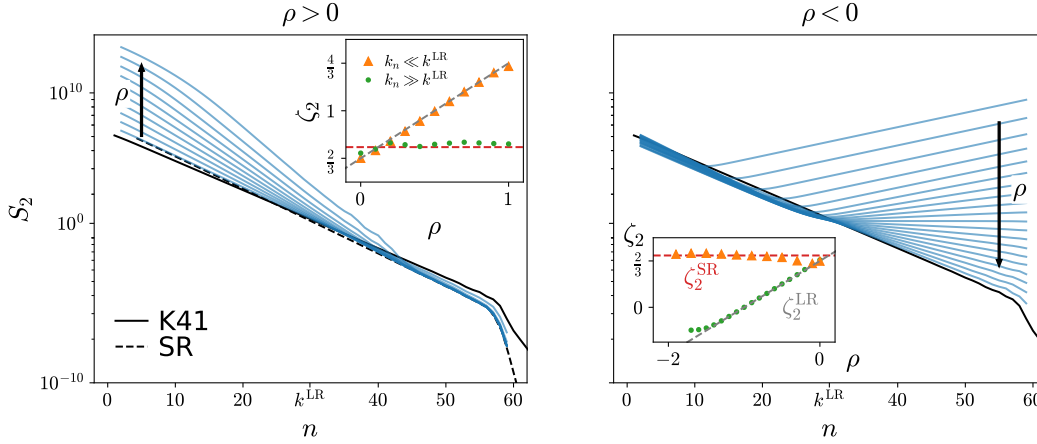


Figure 5: Second order structure function  $S_2$  in the presence of both a SR and a LR forcing for  $0 \leq \rho \leq 1$  (left panel), and for  $-2 \leq \rho \leq 0$  (right panel). The insets show the exponent  $\zeta_2$  for  $k_n \ll k^{\text{LR}}$  (orange symbols) and  $k_n \gg k^{\text{LR}}$  (green symbols), where  $k^{\text{LR}}$  is a crossover wave-number defined as  $k^{\text{LR}} = (D^{\text{LR}}/D)^{1/\rho}$  when  $\rho \neq 0$ . The small shell indices  $k_n < k^{\text{LR}}$ , *i.e.* the inertial range if  $k^{\text{LR}} \gg L^{-1}$ , are controlled by the LR fixed-point for  $\rho > 0$  leading to  $\zeta_2^{\text{LR}} = \frac{2(1+\rho)}{3}$ , whereas they are controlled by the SR fixed-point for  $\rho < 0$  yielding  $\zeta_2^{\text{SR}} \simeq 0.74$ . The case  $\rho = 0$ ,  $D^{\text{LR}}$  finite (black solid line) is denoted K41 since it corresponds to normal scaling, whereas the purely SR case  $D^{\text{LR}} = 0$  (black dashed line) is denoted SR and corresponds to anomalous scaling.

analogue of the limit  $\epsilon \rightarrow 4$  in perturbative RG studies of three-dimensional Navier-Stokes turbulence), one thus exactly recovers K41 scaling, *i.e.*  $\zeta_2^{\text{LR}} = 2/3$ .

Let us notice that at the beginning of the RG flow for  $\kappa \lesssim \Lambda$ , the renormalisation is very weak. In fact, for a pure LR forcing, the flow equations (62), (63), and (64) behave at large  $\kappa$ , *i.e.* when the three functions are close to their initial condition, and  $k_n \sim \kappa$  where the flows are maximal, as:

$$\partial_s f_{\kappa,n}^v \sim \frac{\nu \kappa^2}{(\kappa \eta)^{\rho+4}}, \quad \partial_s f_{\kappa,n}^D \sim \frac{D^{\text{LR}} \kappa^{-\rho}}{(\eta \kappa)^{\rho+4}}, \quad \partial_s f_{\kappa,n}^\lambda \sim \frac{1}{(\eta \kappa)^{\rho+4}}. \quad (48)$$

The right hand sides of these flow equations is suppressed at large  $k_n$  by large powers of  $\kappa \eta$ . The flow becomes non negligible when the RG scale reaches the order of the Kolmogorov scale  $\eta^{-1}$ . Since the flow is frozen by the regulator for all shells with  $k_n \gg \kappa$ , the shells in the dissipation range beyond this scale are almost not affected by the flow, and the three functions  $f_\kappa^v$ ,  $f_\kappa^D$  and  $f_\kappa^\lambda$  for  $k_n \gtrsim \eta^{-1}$  merely reflect their initial condition. As a consequence,  $S_2$  behaves in the dissipation range as

$$S_2(k_n) = \frac{f_{0,n}^D}{2f_{0,n}^v f_{0,n}^\lambda} \stackrel{n \gtrsim \frac{\ln(k_0 \eta)}{\ln \lambda}}{\simeq} \frac{D^{\text{LR}} k_n^{-\rho}}{2\nu k_n^2} \sim k_n^{-(2+\rho)}. \quad (49)$$

This behaviour is clearly observed in Fig 4 for large shell indices. In particular, let us notice in anticipation of the discussion of Sec. 5.4 that for  $\rho = -2$  one obtains a constant.

### 5.3 Interplay between the LR and SR fixed-points

We now restore the SR forcing  $D \neq 0$  (thus the  $\mathcal{R}_\kappa^{\bar{v}^*}$  regulator part), in order to study the interplay between the two fixed-points. We integrate the flow equations with initial conditions where both  $D$  and  $D^{\text{LR}}$  are finite and for different values of  $\rho$ . The flow reaches a fixed-point for all values of  $\rho$ . However, the fixed-point which controls the shells in the inertial range depends on the value of  $\rho$ , as shown in Fig. 5. In this section, we consider  $L^{-1} \ll k^{\text{LR}} \ll k_\eta$ , where  $k^{\text{LR}}$  is defined as  $k^{\text{LR}} = (D^{\text{LR}}/D)^{1/\rho}$  for  $\rho \neq 0$  and corresponds to the typical scale where the SR and LR amplitudes are comparable. When  $k^{\text{LR}} \gg L^{-1}$ , the inertial range comprises shell indices between these two wave-number scales. For  $\rho > 0$ , the LR fixed point dominates at shells in the inertial range  $k_n \ll k^{\text{LR}}$ , and thus the exponent  $\zeta_2^{\text{LR}}$  is observed in this range, whereas for  $\rho < 0$ , the SR fixed-point dominates in the inertial range, and thus the exponent  $\zeta_2^{\text{SR}} \simeq 0.74$  is observed instead.

The small scales  $k_\eta \gg k_n \gg k^{\text{LR}}$  are controlled by the opposite fixed point, since the LR component  $\propto k_n^{-\rho}$  dominates over the SR one for  $\rho < 0$  and is negligible for  $\rho > 0$ . For  $\rho = 0$ , the LR forcing also dominates the inertial range, and the corresponding fixed-point, denoted K41, clearly differs from the purely SR fixed-point, denoted SR. This case is further elucidated in Fig. 4 (right panel). Here we consider the sum of the SR component with amplitude  $D$  and the LR component with  $\rho = 0$  and amplitude  $D^{\text{LR}}$  and we let the ratio  $D/D^{\text{LR}} \rightarrow 0$ . We observe a clear crossover between the SR and LR fixed-points. When  $D^{\text{LR}}/D$  is large, the LR fixed point dominates, whereas when  $D^{\text{LR}}/D$  becomes negligible (smaller than a certain threshold), the SR fixed-point takes over. This crossover results in a two plateaus structure for  $\zeta_2$ , which takes the K41 value  $\zeta_2^{\text{LR}} = 2/3$  at large  $D^{\text{LR}}/D$  and reaches the anomalous value  $\zeta_2^{\text{SR}} \simeq 0.74$  when  $D \rightarrow 0$ . The two types of forcing, LR and SR, thus correspond to two distinct fixed-points, or in other words, they lead to two distinct universality classes. Hence the scaling in the inertial range is universal in the sense that it does not depend on the precise profile of the forcing *as long as it is concentrated at large scale*. But it is altered by the presence of a long-range forcing with  $\rho \geq 0$ , which leads to a different universality class, characterised by non-anomalous exponents.

This has an important consequence for RG calculations of the anomalous exponents. This means that the limit  $\rho \rightarrow 0$  does not suffice to capture the anomalous scaling, the presence of the SR component is mandatory. When it is absent, one finds only the LR fixed-point with K41 scaling at  $\rho = 0$  as demonstrated in Fig. 4. Hence, the strategy followed in perturbative RG approaches which consists in trying to reach the intermittent fixed-point as the limiting case of the LR fixed-point is doomed to fail for the shell model. This provides indications that it is also the case for the Navier-Stokes equation, and strongly suggests that the presence of a large scale forcing is necessary to describe intermittency. This can be achieved using non-perturbative implementations of the RG, such as the FRG used in this work.

### 5.4 Dissipative range and thermal noise

The study of the LR forcing includes as a specific case the presence of a thermal noise, *i.e.* a stochastic component similar to (44) with  $\rho = -2$ , which corresponds to a spectrum  $\propto D^{\text{th}} k_n^2$ , but with a typical scale much smaller than the Kolmogorov scale, *i.e.*  $k^{\text{LR}} \gg k_\eta$ . In this case, it does not represent a forcing but rather a microscopic noise, due to thermal fluctuations. The presence of such fluctuations was argued to affect the properties of the turbulent flow at scales well above the mean-free path, *i.e.* at scales within the dissipation range. Their effect is to alter the form of the spectrum in the dissipation range, replacing the exponential decay expected for Navier-Stokes equation, by an equipartition spectrum  $\propto k^2$  [53–55]. This effect was observed in

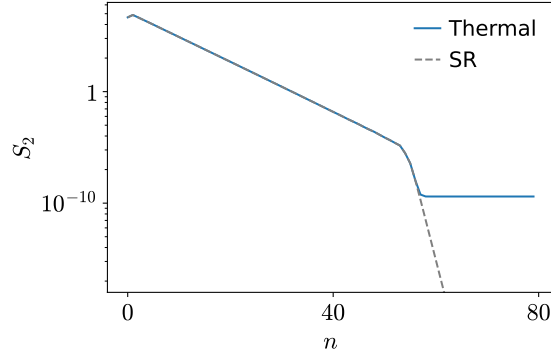


Figure 6: Second order structure function  $S_2$  in the presence of both a SR forcing and a thermal noise with spectrum  $D^{\text{th}}k_n^2$ .

numerical simulations of the Sabra model, which evidenced a crossover in the dissipation range to an equipartition spectrum, *i.e.* a constant in this case.

The Sabra model with thermal noise can be simply studied in the FRG framework by setting  $\rho = -2$  and reducing the Kolmogorov scale such that  $\eta^{-1} \ll k^{\text{LR}}$  in order to resolve the dissipation spectrum. The result is shown in Fig. 6, and is in very close agreement with the direct numerical simulations of the Sabra shell model [53]. The fast decay of the spectrum beyond the Kolmogorov scale is cut out and replaced by the equipartition spectrum.

## 6 Conclusion and perspectives

We presented a FRG analysis of the Sabra shell model of turbulence. Within a simple approximation, called LO, which consists in including a functional renormalisation of the two-point functions while neglecting the renormalisation of higher-order vertices, we obtain the fixed-point corresponding to a forcing concentrated at large scales (small shell indices). We show that this fixed-point is intermittent, it yields anomalous exponents  $\zeta_p$  for the structure functions. Although the value of  $\zeta_2$  is in good agreement with results from simulations, higher-order  $\zeta_p$  are similar, within the LO approximation, to the ones of a  $\beta$ -model, *i.e.* they have an affine dependence on the order  $p$ . Obtaining multi-fractal behaviour requires a richer approximation, which also accounts for the renormalisation of higher-order vertices and/or a functional frequency dependence of the two-point functions.

The FRG framework allowed us to investigate the interplay between a long-range forcing  $\propto k_n^{-\rho}$  and the short-range forcing concentrated at large scales. We show that they correspond to two distinct fixed points: the LR fixed-point has normal scaling  $\zeta_2^{\text{LR}} = 2(1 + \rho)/3$  whereas the SR one is anomalous  $\zeta_2^{\text{SR}} \simeq 0.74$ . When the two types of forcing coexist and compete, the inertial range scaling is dominated by the fixed-point with largest exponent, *i.e.* the LR fixed-point for  $\rho > 0$  and the SR one for  $\rho < 0$ . The important result is that the two fixed-points do not coincide in the limit  $\rho \rightarrow 0$ . It implies that one cannot describe the anomalous SR fixed-point from the limit  $\rho \rightarrow 0$  of the LR one in the absence of a large scale forcing. This conclusion is likely to hold also for Navier-Stokes turbulence, and strongly suggests that one has to include a true large-scale forcing in the RG analysis. Such a large-scale forcing cannot be easily handled within a perturbative RG

framework, but it can be very simply included within the FRG framework.

The numerical integration of the flow equations presented in this work is extremely fast. It is in particular much faster than direct numerical simulation since one does not have to do any averages: the solution of the FRG directly provides the averaged statistical properties of the system. To obtain more accurate results for higher-order exponents  $\zeta_p$  would require a richer approximation, which would then lead to longer computational time to solve the associated FRG equations. It would be extremely interesting to test which level of accuracy on the anomalous exponents can be reached within a still competitive approximation scheme compared to direct numerical simulation. This work opens promising perspectives for the calculation of anomalous exponents in hydrodynamic turbulence from Navier-Stokes equation, since the same type of approximations could be adapted for this case. This work is in progress.

## Acknowledgement

The authors wish to thank N. Wschebor and G. Eyink for stimulating discussions. L.C. acknowledges support from the French ANR through the project NeqFluids (grant ANR-18-CE92-0019) and support from Institut Universitaire de France (IUF). M.T. and E.B. acknowledge support from the Simons Foundation, grant number 663054, through a subagreement from the Johns Hopkins University. The contents of this publication are solely the responsibility of the authors and do not necessarily represent the official views of Simons Foundation or the Johns Hopkins University.

## A Sabra model in the presence of the zero mode

It was proposed in Ref. [12] to modify the shell model equations by introducing a shell zero-mode in order to mimic the sweeping effect present in three-dimensional turbulence. The equations then read

$$\begin{cases} \partial_t v_n = B_n[v, v^*] - ik_n v_\Omega v_n - \nu k_n^2 v_n + f_n \\ \partial_t v_\Omega = f_\Omega, \end{cases} \quad (50)$$

where  $v_\Omega$  and  $f_\Omega$  denote the real shell zero-mode and forcing of the zero-mode respectively. The non-linear term  $B$  is unaltered. This system of equations possesses a Galilean symmetry, contrarily to the original shell model. Indeed, if  $\{(v_n, v_n^*)_{n \in \mathbb{Z}}, v_\Omega\}$  is a solution of (50) with forcing  $\{(f_n, f_n^*)_{n \in \mathbb{Z}}, f_\Omega\}$ , then the Galilean-transformed variables

$$\begin{cases} v_n(t) \rightarrow e^{itV k_n} v_n(t) \\ v_n^*(t) \rightarrow e^{-itV k_n} v_n^*(t) \\ v_\Omega(t) \rightarrow v_\Omega(t) - V, \end{cases} \quad (51)$$

are solutions of the same equations with forcing  $\{(e^{itV k_n} f_n, e^{-itV k_n} f_n^*)_{n \in \mathbb{Z}}, f_\Omega\}$ , for any constant  $V$ . Furthermore, in the absence of forcing the shell variable zero-mode is conserved, in analogy with the total momentum in three-dimensional turbulence. Of course, such a modification is rather artificial and can be completely integrated out due to its linear nature. In the absence of the zero-mode, the shell models are thus free of sweeping.

Let us now show for completeness what are the implications of this symmetry within the Martin-Siggia-Rose field-theoretical framework. To do so, we assume as previously a random



forcing with a Gaussian distribution whose covariance is white in time. The action corresponding to the modified shell model reads

$$\mathcal{S}_{\text{zero-mode}}[V, v_\Omega, \bar{v}_\Omega] = \mathcal{S}[V] + \Delta\mathcal{S}_{L-1}[V] - i \sum_n \int_t k_n v_\Omega \bar{v}_n^* v_n + \text{c.c.} + \int_t (\bar{v}_\Omega \partial_t v_\Omega - N_{L-1}(0) \bar{v}_\Omega^2), \quad (52)$$

where  $\bar{v}_\Omega$  is the response field associated to the dynamics of the zero-mode. The first two terms correspond to the original Sabra model and are identical to the ones given in (13).

Within the field-theoretical framework, the Galilean invariance can be promoted to an extended symmetry, which allows one to derive local exact relations between correlation functions, through Ward identities. We refer to eg Ref. [34, 35] for a detailed presentation of extended symmetries of the Navier-Stokes equations. These identities are at the core of the results obtained from FRG on the form of the time dependence of arbitrary  $n$ -point correlation functions at large wave-numbers, mentioned in Sec. 3. Let us express the (extended) Galilean symmetry for the Sabra shell model in the presence of the zero-mode. For this, we consider an arbitrary function of time  $R(t)$ , and apply the following time-dependent Galilean transformation

$$\begin{cases} v_n(t) \rightarrow e^{iRk_n} v_n(t) \\ \bar{v}_n(t) \rightarrow e^{iRk_n} \bar{v}_n(t) \\ v_\Omega(t) \rightarrow v_\Omega(t) - \partial_t R. \end{cases} \quad (53)$$

One finds that the action is invariant under this transformation up to the following term:

$$\delta\mathcal{S}_{\text{zero-mode}}[V, v_\Omega, \bar{v}_\Omega] = - \int_t \bar{v}_\Omega \partial_t^2 R. \quad (54)$$

As this term is linear in the dynamical fields (in this case,  $\bar{v}_\Omega$ ), it defines the time-dependent Galilean transformation as an extended symmetry. Extended symmetries can be used to derive useful exact identities called Ward identities for the one-particle irreducible functional, or rather in the FRG framework for the effective average action. The Ward identities entail that if an infinitesimal linear transformation is an extended symmetry of the action, then the effective average action transforms as the action. For the time-dependent Galilean transformation, this means

$$\delta\Gamma_\kappa[U, u_\Omega, \bar{u}_\Omega] = \delta\mathcal{S}_{\text{zero-mode}}[U, u_\Omega, \bar{u}_\Omega]. \quad (55)$$

The Ward identity reads explicitly

$$\int_t \left\{ -\partial_t R \frac{\delta\Gamma_\kappa}{\delta u_\Omega} + \sum_n \left( iRk_n u_n \frac{\delta\Gamma_\kappa}{\delta u_n} + iRk_n \bar{u}_n \frac{\delta\Gamma_\kappa}{\delta \bar{u}_n} + \text{c.c.} \right) \right\} = - \int_t \bar{u}_\Omega \partial_t^2 R. \quad (56)$$

This identity can be integrated to write the effective average action in the form

$$\Gamma_\kappa[U, u_\Omega, \bar{u}_\Omega] = \bar{\Gamma}_\kappa[e^{iR\nabla} U, \bar{u}_\Omega] + \int_t \bar{u}_\Omega \partial_t u_\Omega, \quad (57)$$

where  $\bar{\Gamma}_\kappa$  is an arbitrary functional.

Now, let us express the conservation of the zero-mode. We consider an arbitrary function of time  $\bar{V}(t)$  and the shift

$$\bar{v}_\Omega \rightarrow \bar{v}_\Omega + \bar{V}. \quad (58)$$

This shift leaves the action invariant up to the term

$$\delta \mathcal{S}_{\text{zero-mode}}[V, v_\Omega, \bar{v}_\Omega] = \int_t \bar{V} \left\{ \partial_t u_\Omega - 2N_{L-1}(0) \bar{u}_\Omega \right\}, \quad (59)$$

which is again linear in the fields. As we have identified  $N_{L-1}$  with the regulator, the second term in curly braces is absorbed in the definition of the effective average action and we are left with the following Ward identity for the shift of the zero-mode response field:

$$\int_t \bar{V} \frac{\delta \Gamma_\kappa}{\delta \bar{u}_\Omega} = \int_t \bar{V} \partial_t u_\Omega, \quad (60)$$

or, in terms of the parametrisation (57),

$$\Gamma_\kappa[U, u_\Omega, \bar{u}_\Omega] = \bar{\Gamma}_\kappa[e^{i r_\Omega \nabla} U] + \int_t \bar{u}_\Omega \partial_t u_\Omega, \quad (61)$$

where  $\bar{\Gamma}_\kappa$  is an arbitrary functional. This is the more general form of the effective average action compatible with the constraints stemming from the extended symmetries.

## B FRG flow equations in the LO approximation

The computation of the flow equations for the three running functions  $f_\kappa^v$ ,  $f_\kappa^\lambda$  and  $f_\kappa^D$  is straightforward. They can be deduced using the definition (32) from the flow equations for the two-point functions  $\Gamma_\kappa^{(2)}$  which are given by (23). The trace in this equation can be computed using the explicit expressions (33) for the three-point vertices  $\Gamma_\kappa^{(3)}$  and (28) for the propagator  $G_\kappa$ . Since within the LO approximation, the three functions  $f_\kappa^v$ ,  $f_\kappa^\lambda$  and  $f_\kappa^D$  do not depend on the frequency, and neither do the vertices, the only frequency dependence is the bare one in the propagator, so that the frequency integral can be analytically carried out. One finally obtains

$$\begin{aligned} \partial_s f_{\kappa,n}^v &= \frac{k_0^2 \lambda^{2n}}{2} \left[ ab \left( \lambda^2 \Phi_\kappa^v(n+2, n+1) + \Phi_\kappa^v(n+1, n-1) \right) \right. \\ &\quad \left. + ac \left( \lambda^2 \Phi_\kappa^v(n+1, n+2) + \frac{1}{\lambda^2} \Phi_\kappa^v(n-1, n-2) \right) + bc \left( \Phi_\kappa^v(n-1, n+1) + \frac{1}{\lambda^2} \Phi_\kappa^v(n-2, n-1) \right) \right] \end{aligned} \quad (62)$$

$$\begin{aligned} \partial_s f_{\kappa,n}^\lambda &= \frac{k_0^2 \lambda^{2n}}{2} \left[ ab \left( \lambda^2 \Phi_\kappa^\lambda(n+2, n+1) + \Phi_\kappa^\lambda(n+1, n-1) \right) \right. \\ &\quad \left. + ac \left( \lambda^2 \Phi_\kappa^\lambda(n+1, n+2) + \frac{1}{\lambda^2} \Phi_\kappa^\lambda(n-1, n-2) \right) + bc \left( \Phi_\kappa^\lambda(n-1, n+1) + \frac{1}{\lambda^2} \Phi_\kappa^\lambda(n-2, n-1) \right) \right] \end{aligned} \quad (63)$$

$$\partial_s f_{\kappa,n}^D = \frac{k_0^2 \lambda^{2n}}{2} \left[ a^2 \lambda^2 \Phi_\kappa^D(n+1, n+2) + b^2 \Phi_\kappa^D(n-1, n+1) + \frac{c^2}{\lambda^2} \Phi_\kappa^D(n-2, n-1) \right] \quad (64)$$

where we have defined

$$\begin{aligned}
\Phi_{\kappa}^{\nu}(i, j) &= \frac{\tilde{f}_{\kappa,i}^D \left( \dot{R}_{\kappa,j} f_{\kappa,i}^{\lambda} + \dot{R}_{\kappa,i} f_{\kappa,j}^{\lambda} \left( 2 + \frac{f_{\kappa,i}^{\lambda} \tilde{f}_{\kappa,j}^{\nu}}{f_{\kappa,j}^{\lambda} \tilde{f}_{\kappa,i}^{\nu}} \right) \right)}{\tilde{f}_{\kappa,i}^{\nu} (\tilde{f}_{\kappa,i}^{\nu} f_{\kappa,j}^{\lambda} + \tilde{f}_{\kappa,j}^{\nu} f_{\kappa,i}^{\lambda})^2} - \frac{\dot{N}_{\kappa,i}}{\tilde{f}_{\kappa,i}^{\nu} (\tilde{f}_{\kappa,i}^{\nu} f_{\kappa,j}^{\lambda} + \tilde{f}_{\kappa,j}^{\nu} f_{\kappa,i}^{\lambda})} \\
\Phi_{\kappa}^{\lambda}(i, j) &= \frac{f_{\kappa,i}^{\lambda} f_{\kappa,j}^{\lambda}}{\tilde{f}_{\kappa,i}^{\nu} (\tilde{f}_{\kappa,i}^{\nu} f_{\kappa,j}^{\lambda} + \tilde{f}_{\kappa,j}^{\nu} f_{\kappa,i}^{\lambda})^2} \left( \frac{2\dot{R}_{\kappa,j} \tilde{f}_{\kappa,i}^D f_{\kappa,i}^{\lambda} + \dot{R}_{\kappa,i} \tilde{f}_{\kappa,j}^D f_{\kappa,j}^{\lambda} \left( 3 + \frac{f_{\kappa,i}^{\lambda} \tilde{f}_{\kappa,j}^{\nu}}{f_{\kappa,j}^{\lambda} \tilde{f}_{\kappa,i}^{\nu}} \right)}{\tilde{f}_{\kappa,i}^{\nu} f_{\kappa,j}^{\lambda} + \tilde{f}_{\kappa,j}^{\nu} f_{\kappa,i}^{\lambda}} - \dot{N}_{\kappa,i} \right) \\
\Phi_{\kappa}^D(i, j) &= \frac{\dot{N}_{\kappa,j} \tilde{f}_{\kappa,i}^D + \dot{N}_{\kappa,i} \tilde{f}_{\kappa,j}^D}{\tilde{f}_{\kappa,i}^{\nu} \tilde{f}_{\kappa,j}^{\nu} (f_{\kappa,j}^{\lambda} \tilde{f}_{\kappa,i}^{\nu} + f_{\kappa,i}^{\lambda} \tilde{f}_{\kappa,j}^{\nu})} - \frac{\tilde{f}_{\kappa,i}^D \tilde{f}_{\kappa,j}^D \left( \dot{R}_{\kappa,j} f_{\kappa,i}^{\lambda} \left( 2 + \frac{\tilde{f}_{\kappa,i}^{\nu} f_{\kappa,j}^{\lambda}}{\tilde{f}_{\kappa,j}^{\nu} f_{\kappa,i}^{\lambda}} \right) + \dot{R}_{\kappa,i} f_{\kappa,j}^{\lambda} \left( 2 + \frac{\tilde{f}_{\kappa,j}^{\nu} f_{\kappa,i}^{\lambda}}{\tilde{f}_{\kappa,i}^{\nu} f_{\kappa,j}^{\lambda}} \right) \right)}{\tilde{f}_{\kappa,i}^{\nu} \tilde{f}_{\kappa,j}^{\nu} (f_{\kappa,j}^{\lambda} \tilde{f}_{\kappa,i}^{\nu} + f_{\kappa,i}^{\lambda} \tilde{f}_{\kappa,j}^{\nu})^2} \quad (65)
\end{aligned}$$

and introduced the following notations for the functions:

$$\tilde{f}_{\kappa,n}^{\nu} = f_{\kappa,n}^{\nu} + R_{\kappa,n}, \quad \tilde{f}_{\kappa,n}^D = f_{\kappa,n}^D + N_{\kappa,n} \quad (66)$$

and for the derivative of the regulator:

$$\dot{N}_{\kappa,n} = -2D \left( \frac{k_n}{\kappa} \right)^2 \left( 1 + \left( \frac{k_n}{\kappa} \right)^2 \partial_{x^2} \right) n \left( \left( \frac{k_n}{\kappa} \right)^2 \right), \quad \dot{R}_{\kappa,n} = -2\nu k_n^2 \left( \frac{k_n}{\kappa} \right)^2 \partial_{x^2} r \left( \left( \frac{k_n}{\kappa} \right)^2 \right). \quad (67)$$

The RG time  $s$  is defined as  $s = \log \frac{\kappa}{\Lambda}$ . Note that all these flow equations are real for real functions and regulators. Thus, if one starts at  $\kappa = \Lambda$  with real functions, they remain real along the flow.

## C Numerical integration of the flow equations

In this appendix, we provide the details of the numerical integration of the flow equations for the three functions  $f_{\kappa,n}^{\nu}$ ,  $f_{\kappa,n}^D$  and  $f_{\kappa,n}^{\lambda}$ , which are a set of coupled ordinary differential equations. The chosen ODE integrator is the standard function `solve_ivp` of the scientific computing library `scipy`, using a Runge-Kutta of order 4 (method) and 5 (error estimator). The source code of our solver is available in [this repository](#).

A maximum time step of  $\delta\kappa = 10^{-3}$  was sufficient to ensure convergence of the integration scheme. We checked the convergence of the scheme using different time stepping. We considered  $N = 80$  shells between  $n_{\min} = 0$  and  $n_{\max} = 79$  corresponding to the wave-numbers  $k_n = k_0 \lambda^n$  with  $\lambda = 2$  and  $k_0 = 10^{-15}$ . The choice of  $\lambda$  corresponds to the most studied one, as it yields anomalous exponents very similar to the ones for Navier-Stokes turbulence. The value of  $k_0$  is chosen in order to capture a reasonable range in each regimes (inertial and dissipative). The other parameters were chosen in all runs as  $\nu = 10^{-5}$ ,  $D = 10^{-5}$ , which corresponds, in the absence of long-range forcing, to a Kolmogorov scale  $\eta^{-1} = \left( \frac{\varepsilon}{\nu^3} \right)^{\frac{1}{4}} = 291$  and to an injected energy of  $\varepsilon = 0.72D = 7.2 \times 10^{-6}$ , where  $\varepsilon = \sum_n N_{n,\kappa}$  is independent of  $\kappa$ . Let us now specify the boundary conditions. Since the flow equations couple neighbouring shells and since we truncate at a finite number of shells, we need to prescribe the values of the functions on the shells at the external boundary of the integration grid. In order to do so, we assume a power law behaviour for the running functions at large wave-numbers. This is motivated by the expected behaviour

at the fixed-point. Hence, we extrapolate each running function  $f_{\kappa}^X$  for each RG step  $\kappa$ , using logarithmic finite differences at the boundary point

$$\zeta^X = f_{\kappa,N}^X - f_{\kappa,N-1}^X \quad (68)$$

and we fix the value of the sequence at  $n > N$  following

$$f_{\kappa,n}^X = f_{\kappa,N}^X \lambda^{\zeta^X(n-N)}. \quad (69)$$

This principle is also used to extrapolate the value of the functions at shell indices smaller than  $n = 1$ . In the case of the long range forcing, we chose  $k^{\text{LR}} = \left(\frac{D^{\text{LR}}}{D}\right)^{\frac{1}{\rho}} = 10^{-3}$ . Since the flow is computed with fully dimensional quantities, we must also specify a starting and a finishing RG scale. For every run, we chose  $\Lambda = 2^4 \times k_N$ , and  $\kappa_0$ , the final RG scale, as  $\kappa_0 = 2^{-4} \times k_0$ . We checked that this choice has no influence on the results presented in this paper.

## D Dependence on the regulator

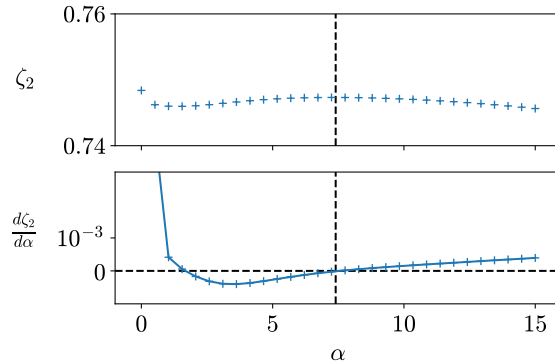


Figure 7: Variations of  $\zeta_2$  with the cut-off parameter  $\alpha$ . The vertical dashed line indicates the optimal parameter  $\alpha_{\text{opt}}$  which corresponds to a minimum. The optimal value for  $\zeta_2$  is obtained as  $\zeta_{2,\text{opt}} = \zeta_2(\alpha_{\text{opt}})$ . The overall variation of  $\zeta_2$  with  $\alpha$  is smaller than the numerical error associated with the fitting procedure.

In order to estimate an error within the LO approximation, a standard procedure within the FRG framework is to study the dependence of the results with respect to the choice of the cut-off function. Indeed, if no approximation is performed, then the exact result does not depend on the choice of the cut-off function since the regulator vanishes in the limit  $\kappa \rightarrow 0$ . However, any approximation introduces a spurious dependence on this choice, which can be used to optimise the accuracy of the results and estimate an error [30, 56, 57]. The best result within a given approximation can be determined from the principle of minimal sensitivity, which consists in searching for a stationary point with respect to the parameters of the cut-off. In this work, we varied the parameter  $\alpha$  defined in (17) and computed the variations of  $\zeta_2$  with respect to  $\alpha$ . The results are presented in Fig. 2. One observes that the overall variation of  $\zeta_2$  is very small. A stationary point is attained for  $\alpha_{\text{opt}} \simeq 7.4$ , which leads to the optimal value  $\zeta_{2,\text{opt}} \simeq 0.743 \pm 0.002$ , where

the error bars correspond to the variation of  $\zeta_2$  in the range  $[\alpha_{\text{opt}}/2, 2\alpha_{\text{opt}}]$ . This error is hence much smaller than the one from the error due to the numerical integration of the flow equations. The error bars given in the main text thus reflect the latter.

## E Structure functions of higher order

In this section, we provide the expression of the structure functions of order higher than three. We consider the fourth order structure function defined in Eq. (43), which is non-zero within the LO approximation. After performing all the frequency integrals, we obtain the following expression



The fifth order structure function defined by the general expression Eq. (7) is non-zero at LO, and given by the following expression:

$$\begin{aligned}
 S_5(k_n) &= \frac{\delta^5 \mathcal{W}}{\delta j_{n-1}(t) j_n(t) j_{n+1}^*(t) j_n(t) j_n^*(t)} = \\
 &\sum_{m_i} \sum_{\beta_i} \int_{\omega_i} \left[ \tilde{G}_{\kappa, n+1}^{u^* U_{\beta_1}}(\omega_1) \tilde{G}_{\kappa, n}^{u U_{\beta_2}}(\omega_2) \tilde{\Gamma}_{\kappa, n+1 n m_1}^{U_{\beta_1} U_{\beta_2} U_{\beta_3}} \tilde{G}_{\kappa, m_1}^{U_{\beta_3} U_{\beta_4}}(\omega_1 + \omega_2) \tilde{G}_{\kappa, n}^{u^* U_{\beta_5}}(\omega_3) \tilde{\Gamma}_{\kappa, m_1 n m_2}^{U_{\beta_4} U_{\beta_5} U_{\beta_6}} \right. \\
 &\quad \times \tilde{G}_{\kappa, m_2}^{U_{\beta_6} U_{\beta_7}}(\omega_1 + \omega_2 + \omega_3) \tilde{\Gamma}_{\kappa, m_2 n n-1}^{U_{\beta_7} U_{\beta_8} U_{\beta_9}} \tilde{G}_{\kappa, n}^{u U_{\beta_8}}(\omega_4) \tilde{G}_{\kappa, n-1}^{u U_{\beta_9}}(-\sum_i \omega_i) \\
 &\quad + \tilde{G}_{\kappa, n+1}^{u^* U_{\beta_1}}(\omega_1) \tilde{G}_{\kappa, n}^{u U_{\beta_2}}(\omega_2) \tilde{\Gamma}_{\kappa, n+1 n m_1}^{U_{\beta_1} U_{\beta_2} U_{\beta_3}} \tilde{G}_{\kappa, m_1}^{U_{\beta_3} U_{\beta_4}}(\omega_1 + \omega_2) \tilde{G}_{\kappa, n}^{u U_{\beta_5}}(\omega_3) \tilde{\Gamma}_{\kappa, m_1 n m_2}^{U_{\beta_4} U_{\beta_5} U_{\beta_6}} \\
 &\quad \times \tilde{G}_{\kappa, m_2}^{U_{\beta_6} U_{\beta_7}}(\omega_1 + \omega_2 + \omega_3) \tilde{\Gamma}_{\kappa, m_2 n n-1}^{U_{\beta_7} U_{\beta_8} U_{\beta_9}} \tilde{G}_{\kappa, n}^{u^* U_{\beta_8}}(\omega_4) \tilde{G}_{\kappa, n-1}^{u U_{\beta_9}}(-\sum_i \omega_i) \\
 &\quad + \tilde{G}_{\kappa, n+1}^{u^* U_{\beta_1}}(\omega_1) \tilde{G}_{\kappa, n}^{u^* U_{\beta_2}}(\omega_2) \tilde{\Gamma}_{\kappa, n+1 n m_1}^{U_{\beta_1} U_{\beta_2} U_{\beta_3}} \tilde{G}_{\kappa, m_1}^{U_{\beta_3} U_{\beta_4}}(\omega_1 + \omega_2) \tilde{G}_{\kappa, n}^{u U_{\beta_5}}(\omega_3) \tilde{\Gamma}_{\kappa, m_1 n m_2}^{U_{\beta_4} U_{\beta_5} U_{\beta_6}} \\
 &\quad \times \tilde{G}_{\kappa, m_2}^{U_{\beta_6} U_{\beta_7}}(\omega_1 + \omega_2 + \omega_3) \tilde{\Gamma}_{\kappa, m_2 n n-1}^{U_{\beta_7} U_{\beta_8} U_{\beta_9}} \tilde{G}_{\kappa, n}^{u U_{\beta_8}}(\omega_4) \tilde{G}_{\kappa, n-1}^{u U_{\beta_9}}(-\sum_i \omega_i) \quad . \quad (71)
 \end{aligned}$$

The explicit expression in terms of the three functions  $f_\kappa^\nu$ ,  $f_\kappa^D$  and  $f_\kappa^\lambda$  is too lengthy to be reported here, but its derivation is straightforward using the LO expressions for the propagator and three-point vertices.

## F Constraints from translational invariance on 4-point configurations

In this appendix, we provide a complete classification of the four-points configuration permitted by the conservation of the quasi-momentum. The rule of conservation of the quasi-momentum is as follows: to each shell variable (respectively their complex conjugate) of shell index  $n$  we associate the quasi-momentum  $\kappa_n = \varphi^n$  (resp.  $\kappa_n = -\varphi^n$ ), where

$$\varphi = \frac{1 + \sqrt{5}}{2}, \quad (72)$$

is the golden mean. The sum of all quasi-momenta in a configuration must be zero for it to preserve the quasi-momentum conservation law. A generic  $p$ -point configuration is given by the data of  $p$  shell indices  $n_1, \dots, n_p \in \mathbb{Z}$  and  $p$  conjugation indices  $\epsilon_1, \dots, \epsilon_p \in \{-1, 1\}$  such that

$$\sum_{i=1}^p \epsilon_i \varphi^{n_i} = 0. \quad (73)$$

When two shell variables have the same shell index and opposite conjugation indices, their quasi-momentum cancel each other. Let us discard from the onset such trivial configurations. Without loss of generality, we can assume furthermore that  $\min_i n_i = 0$ . Then, a configuration containing no trivial cancellations is equivalent to the data of a polynomial  $P = a_{d+2} X^{d+2} + a_{d+1} X^{d+1} + \dots + a_0 \in \mathbb{Z}[X]$  where each  $a_i$  has its sign (resp. its absolute value) given by the conjugation index (resp. the multiplicity) of the shell variables at the given shell index. Consequently, the  $\ell_1$ -norm of  $P$ , given by  $\|P\|_1 = \sum_{i=0}^{d+2} |a_i|$  is equal to the number of points in the configuration. Let us remark also that



by assumption,  $a_0 \neq 0$ . Furthermore, the polynomial degree,  $d + 2$ , gives the total extend of the configuration, *i.e.* the difference between the largest and smallest shell indices. Finally, the configuration conserves the quasi-momentum iff  $\varphi$  is a zero of  $P$ . Thus, we deduce that a configuration conserves the quasi-momentum iff the polynomial  $X^2 - X - 1$  divides  $P$ , *i.e.* there exists  $Q = b_d X^d + b_{d-1} X^{d-1} + \dots + b_0 \in \mathbb{Z}[X]$  such that

$$P = (X^2 - X - 1)Q. \quad (74)$$

In terms of polynomial coefficients, this is equivalent to the following equalities

$$a_i = b_{i-2} - b_{i-1} - b_i, \quad (75)$$

for all  $0 \leq i \leq d + 2$ , with the understanding that in the above expression  $b_{i>d} = b_{i<0} = 0$ . This recurrence relation can be solved to give the following constraints on the  $a_i$ 's:

$$\begin{cases} \sum_{i=0}^{d+1} (-1)^i F_{d+2-i} a_i = 0, \\ \sum_{i=0}^{d+2} (-1)^i F_{d+3-i} a_i = 0, \end{cases} \quad (76)$$

where the  $F_i$ 's are the Fibonacci numbers ( $F_1 = F_2 = 1$  and  $F_i = F_{i-1} + F_{i-2}$ ).

Let us now use these constraints to classify all 4-point configurations. First, we remark that a 4-point configuration must realise one of the following partition of 4: either  $(1, 1, 1, 1)$  or  $(2, 1, 1)$ . Indeed, the partition of 4 into the sum of either one or two integers are prohibited by the fact that both  $a_{d+2}$  and  $a_0$  are non-zero and the first line of (76). Let us consider the case  $(2, 1, 1)$ : there exists a  $a_i \neq 0$  with  $0 < i < d + 2$  and  $a_j = 0$  for  $j \neq 0, i, d + 2$ . The constraints (76) then read

$$\begin{cases} F_{d+2} a_0 + (-1)^i F_{d+2-i} a_i = 0, \\ F_{d+3} a_0 + (-1)^i F_{d+3-i} a_i + (-1)^d a_{d+2} = 0. \end{cases} \quad (77)$$

The first line is satisfied if either  $|a_0| = |a_i| = 1$ , then  $d = 0$  and  $i = 1$ , or if  $|a_0| = 1$  and  $|a_i| = 2$ , then  $d = 1$  and  $i \in \{1, 2\}$ . The choice  $d = 0$  cannot satisfy the second line, so we are left with the choice  $d = 1$ . We find that two configurations conserve the quasi-momentum:

$$\begin{cases} i = 1: & P = X^3 - 2X - 1 \\ i = 2: & P = X^3 - 2X^2 + 1. \end{cases} \quad (78)$$

We now turn to the case  $(1, 1, 1, 1)$ : there exist  $|a_i| = 1$  and  $|a_j| = 1$  with  $0 < i < j < d + 2$  and  $a_k = 0$  for  $k \neq 0, i, j, d + 2$ . The constraints (76) then read

$$\begin{cases} F_{d+2} a_0 + (-1)^i F_{d+2-i} a_i + (-1)^j F_{d+2-j} a_j = 0, \\ F_{d+3} a_0 + (-1)^i F_{d+3-i} a_i + (-1)^j F_{d+3-j} a_j + (-1)^d a_{d+2} = 0. \end{cases} \quad (79)$$

From the first line, we deduce that either  $i = 1$  and  $j = 2$ , for any  $d$ , or that  $i = 1$ ,  $j = 3$ , and then  $d = 2$ . Using the second line, the first possibility leads to the contradiction  $a_{d+2} = 0$ , so we are left with the second possibility. We find that the following configuration conserves the quasi-momentum:

$$P = X^4 - X^3 - X - 1. \quad (80)$$

To sum up, we illustrate the possible 4-point configurations which preserve the quasi-momentum by listing all fourth moments of the shell variable, up to a global conjugation, compatible with translational invariance:

$$\langle u_m u_m^* u_n u_n^* \rangle, \quad \langle u_{n+3} (u_{n+1}^*)^2 u_n^* \rangle, \quad \langle u_{n+3} (u_{n+2}^*)^2 u_n \rangle, \quad \langle u_{n+4} u_{n+3}^* u_{n+1}^* u_n^* \rangle. \quad (81)$$

## References

- [1] U. Frisch, *Turbulence: the legacy of A. N. Kolmogorov*, Cambridge University Press, Cambridge, doi:[10.1017/CBO9781139170666](https://doi.org/10.1017/CBO9781139170666) (1995).
- [2] A. N. Kolmogorov, *The local structure of turbulence in incompressible viscous fluid for very large Reynolds number*, Dokl. Akad. Nauk SSSR **30**, 299 (1941).
- [3] A. N. Kolmogorov, *Dissipation of energy in locally isotropic turbulence*, Dokl. Akad. Nauk SSSR **32**, 16 (1941).
- [4] J. Burgers, *A mathematical model illustrating the theory of turbulence*, vol. 1 of *Advances in Applied Mechanics*, pp. 171–199. Elsevier, doi:[https://doi.org/10.1016/S0065-2156\(08\)70100-5](https://doi.org/10.1016/S0065-2156(08)70100-5) (1948).
- [5] P. Constantin, P.D. Lax and A. Majda, *A simple one-dimensional model for the three-dimensional vorticity equation*, Communications on Pure and Applied Mathematics **38**(6), 715 (1985), doi:<https://doi.org/10.1002/cpa.3160380605>, <https://onlinelibrary.wiley.com/doi/pdf/10.1002/cpa.3160380605>.
- [6] L. Biferale, *Shell models of energy cascade in Turbulence*, <http://dx.doi.org/10.1146/annurev.fluid.35.101101.161122> (2003), doi:[10.1146/annurev.fluid.35.101101.161122](https://doi.org/10.1146/annurev.fluid.35.101101.161122).
- [7] P. D. Ditlevsen, *Turbulence and Shell Models*, Cambridge University Press, Cambridge, UK ; New York, ISBN 978-0-521-19036-7 (2011).
- [8] E. B. Gledzer, *System of hydrodynamic type admitting two quadratic integrals of motion*, Sov. Phys. Dokl. **18**, 216 (1973).
- [9] V. N. Desnyansky and E. A. Novikov, *The evolution of turbulence spectra to the similarity regime*, Izv. Akad. Nauk. SSSR Fiz. Atmos. Okeana **10**, 127 (1974).
- [10] E. D. Siggia, *Model of intermittency in three-dimensional turbulence*, Phys. Rev. A **17**, 1166 (1978), doi:[10.1103/PhysRevA.17.1166](https://doi.org/10.1103/PhysRevA.17.1166).
- [11] A. A. Mailybaev, *Continuous representation for shell models of turbulence*, Nonlinearity **28**(7), 2497 (2015), doi:[10.1088/0951-7715/28/7/2497](https://doi.org/10.1088/0951-7715/28/7/2497).
- [12] C. S. Campolina and A. A. Mailybaev, *Fluid dynamics on logarithmic lattices*, Nonlinearity **34**(7), 4684 (2021), doi:[10.1088/1361-6544/abef73](https://doi.org/10.1088/1361-6544/abef73).
- [13] M. Yamada and K. Ohkitani, *The Inertial Subrange and Non-Positive Lyapunov Exponents in Fully-Developed Turbulence*, Progress of Theoretical Physics **79**(6), 1265 (1988), doi:[10.1143/PTP79.1265](https://doi.org/10.1143/PTP79.1265).
- [14] T. Dombre and J.-L. Gilson, *Intermittency, chaos and singular fluctuations in the mixed Obukhov-Novikov shell model of turbulence*, Physica D: Nonlinear Phenomena **111**(1), 265 (1998), doi:[10.1016/S0167-2789\(97\)80015-2](https://doi.org/10.1016/S0167-2789(97)80015-2).

- [15] V. S. L'Vov, E. Podivilov, A. Pomyalov, I. Procaccia and D. Vandembroucq, *Improved shell model of turbulence*, Phys. Rev. E - Stat. Phys. Plasmas Fluids Relat. Interdiscip. Top. **58**(2), 1811 (1998), doi:[10.1103/PhysRevE.58.1811](https://doi.org/10.1103/PhysRevE.58.1811).
- [16] G. L. Eyink, *Large- $N$  limit of the “spherical model” of turbulence*, Phys. Rev. E **49**, 3990 (1994), doi:[10.1103/PhysRevE.49.3990](https://doi.org/10.1103/PhysRevE.49.3990).
- [17] Pierotti, D., *Intermittency in the large- $n$  limit of a spherical shell model for turbulence*, Europhys. Lett. **37**(5), 323 (1997), doi:[10.1209/epl/i1997-00151-4](https://doi.org/10.1209/epl/i1997-00151-4).
- [18] V. S. L'Vov, E. Podivilov and I. Procaccia, *Hamiltonian structure of the Sabra shell model of turbulence: Exact calculation of an anomalous scaling exponent*, Europhys. Lett. **46**(5), 609 (1999), doi:[10.1209/epl/i1999-00307-8](https://doi.org/10.1209/epl/i1999-00307-8).
- [19] A. A. Mailybaev, *Solvable Intermittent Shell Model of Turbulence*, Commun. Math. Phys. (2) (2021), doi:[10.1007/s00220-021-04190-z](https://doi.org/10.1007/s00220-021-04190-z).
- [20] K. G. Wilson and J. Kogut, *The Renormalization Group and the  $\epsilon$ -expansion*, Phys. Rep. C **12**, 75 (1974).
- [21] D. Forster, D. R. Nelson and M. J. Stephen, *Large-distance and long-time properties of a randomly stirred fluid*, Phys. Rev. A **16**(2), 732 (1977), doi:[10.1103/PhysRevA.16.732](https://doi.org/10.1103/PhysRevA.16.732).
- [22] C. DeDominicis and P. C. Martin, *Energy spectra of certain randomly-stirred fluids*, Phys. Rev. A **19**, 419 (1979), doi:[10.1103/PhysRevA.19.419](https://doi.org/10.1103/PhysRevA.19.419).
- [23] J. D. Fournier and U. Frisch, *Remarks on the renormalization group in statistical fluid dynamics*, Phys. Rev. A **28**, 1000 (1983), doi:[10.1103/PhysRevA.28.1000](https://doi.org/10.1103/PhysRevA.28.1000).
- [24] L. Smith and S. Woodruff, *Renormalization Group analysis of turbulence*, Annu. Rev. Fluid Mech. **30**, 275 (1998).
- [25] L. T. Adzhemyan, N. V. Antonov and A. N. Vasil'ev, *The Field Theoretic Renormalization Group in Fully Developed Turbulence*, Gordon and Breach, London (1999).
- [26] Y. Zhou, *Renormalization Group theory for fluid and plasma turbulence*, Phys. Rep. **488**(1), 1 (2010), doi:[10.1016/j.physrep.2009.04.004](https://doi.org/10.1016/j.physrep.2009.04.004).
- [27] J. Berges, N. Tetradis and C. Wetterich, *Non-perturbative Renormalization flow in quantum field theory and statistical physics*, Phys. Rep. **363**(4-6), 223 (2002), doi:[DOI:10.1016/S0370-1573\(01\)00098-9](https://doi.org/10.1016/S0370-1573(01)00098-9), [hep-ph/0005122](https://arxiv.org/abs/hep-ph/0005122).
- [28] P. Kopietz, L. Bartosch and F. Schütz, *Introduction to the Functional Renormalization Group*, vol. 798 of *Lecture Notes in Physics*, Springer, Berlin, doi:<https://doi.org/10.1007/978-3-642-05094-7> (2010).
- [29] B. Delamotte, *An Introduction to the nonperturbative renormalization group*, Lect. Notes Phys. **852**, 49 (2012), doi:[10.1007/978-3-642-27320-9\\_2](https://doi.org/10.1007/978-3-642-27320-9_2), [cond-mat/0702365](https://arxiv.org/abs/cond-mat/0702365).
- [30] N. Dupuis, L. Canet, A. Eichhorn, W. Metzner, J. Pawłowski, M. Tissier and N. Wschebor, *The nonperturbative functional renormalization group and its applications*, Physics Reports **910**, 1 (2021), doi:<https://doi.org/10.1016/j.physrep.2021.01.001>, The nonperturbative functional renormalization group and its applications.

- [31] P. Tomassini, *An exact renormalization group analysis of 3d well developed turbulence*, Physics Letters B **411**(1), 117 (1997), doi:[10.1016/S0370-2693\(97\)00980-5](https://doi.org/10.1016/S0370-2693(97)00980-5).
- [32] C. Mejía-Monasterio and P. Muratore-Ginanneschi, *Nonperturbative Renormalization Group study of the stochastic Navier-Stokes equation*, Phys. Rev. E **86**, 016315 (2012), doi:[10.1103/PhysRevE.86.016315](https://doi.org/10.1103/PhysRevE.86.016315).
- [33] L. Canet, B. Delamotte and N. Wschebor, *Fully developed isotropic turbulence: Nonperturbative renormalization group formalism and fixed-point solution*, Phys. Rev. E **93**, 063101 (2016), doi:[10.1103/PhysRevE.93.063101](https://doi.org/10.1103/PhysRevE.93.063101).
- [34] L. Canet, *Spatio-temporal correlations in turbulence from functional renormalisation group*, J. Fluid Mech. Perspectives (arXiv:2205.01427).
- [35] M. Tarpin, L. Canet and N. Wschebor, *Breaking of scale invariance in the time dependence of correlation functions in isotropic and homogeneous turbulence*, Physics of Fluids **30**(5), 055102 (2018), doi:[10.1063/1.5020022](https://doi.org/10.1063/1.5020022), <https://doi.org/10.1063/1.5020022>.
- [36] L. Canet, V. Rossetto, N. Wschebor and G. Balarac, *Spatiotemporal velocity-velocity correlation function in fully developed turbulence*, Phys. Rev. E **95**, 023107 (2017), doi:[10.1103/PhysRevE.95.023107](https://doi.org/10.1103/PhysRevE.95.023107).
- [37] A. Gorbunova, G. Balarac, L. Canet, G. Eyink and V. Rossetto, *Spatio-temporal correlations in three-dimensional homogeneous and isotropic turbulence*, Physics of Fluids **33**(4), 045114 (2021), doi:[10.1063/5.0046677](https://doi.org/10.1063/5.0046677), <https://doi.org/10.1063/5.0046677>.
- [38] C. Pagani and L. Canet, *Spatio-temporal correlation functions in scalar turbulence from functional renormalization group*, Physics of Fluids **33**(6), 065109 (2021), doi:[10.1063/5.0050515](https://doi.org/10.1063/5.0050515).
- [39] A. Gorbunova, C. Pagani, G. Balarac, L. Canet and V. Rossetto, *Eulerian spatiotemporal correlations in passive scalar turbulence*, Phys. Rev. Fluids **6**, 124606 (2021), doi:[10.1103/PhysRevFluids.6.124606](https://doi.org/10.1103/PhysRevFluids.6.124606).
- [40] G. L. Eyink, *Renormalization group and operator product expansion in turbulence: Shell models*, Phys. Rev. E **48**(3), 1823 (1993), doi:[10.1103/PhysRevE.48.1823](https://doi.org/10.1103/PhysRevE.48.1823).
- [41] U. Frisch, P.-L. Sulem and M. Nelkin, *A simple dynamical model of intermittent fully developed turbulence*, Journal of Fluid Mechanics **87**(4), 719–736 (1978), doi:[10.1017/S0022112078001846](https://doi.org/10.1017/S0022112078001846).
- [42] A. Sain, Manu and R. Pandit, *Turbulence and multiscaling in the randomly forced Navier-Stokes equation*, Phys. Rev. Lett. **81**, 4377 (1998), doi:[10.1103/PhysRevLett.81.4377](https://doi.org/10.1103/PhysRevLett.81.4377).
- [43] L. Biferale, A. S. Lanotte and F. Toschi, *Effects of forcing in three-dimensional turbulent flows*, Phys. Rev. Lett. **92**, 094503 (2004), doi:[10.1103/PhysRevLett.92.094503](https://doi.org/10.1103/PhysRevLett.92.094503).
- [44] L. Biferale, M. Cencini, A. S. Lanotte, M. Sbragaglia and F. Toschi, *Anomalous scaling and universality in hydrodynamic systems with power-law forcing*, New Journal of Physics **6**, 37 (2004), doi:[10.1088/1367-2630/6/1/037](https://doi.org/10.1088/1367-2630/6/1/037).

- [45] P. C. Martin, E. D. Siggia and H. A. Rose, *Statistical dynamics of classical systems*, Phys. Rev. A **8**, 423 (1973), doi:[10.1103/PhysRevA.8.423](https://doi.org/10.1103/PhysRevA.8.423).
- [46] H.-K. Janssen, *On a Lagrangean for classical field dynamics and Renormalization Group calculations of dynamical critical properties*, Z. Phys. B **23**, 377 (1976), doi:[10.1007/BF01316547](https://doi.org/10.1007/BF01316547).
- [47] C. de Dominicis, *Techniques de renormalisation de la théorie des champs et dynamique des phénomènes critiques*, J. Phys. (Paris) Colloq. **37**(C1), 247 (1976), doi:[10.1051/jphyscol:1976138](https://doi.org/10.1051/jphyscol:1976138).
- [48] G. L. Eyink, *The renormalization group method in statistical hydrodynamics*, Physics of Fluids **6**(9), 3063 (1994), doi:[10.1063/1.868131](https://doi.org/10.1063/1.868131).
- [49] D. Barbi and G. Münster, *Renormalisation group analysis of turbulent hydrodynamics*, Physics Research International **2013**, 872796 (2013), doi:[10.1155/2013/872796](https://doi.org/10.1155/2013/872796).
- [50] M. Tarpin, L. Canet, C. Pagani and N. Wschebor, *Stationary, isotropic and homogeneous two-dimensional turbulence: a first non-perturbative renormalization group approach*, Journal of Physics A: Mathematical and Theoretical **52**(8), 085501 (2019), doi:[10.1088/1751-8121/aaf3f0](https://doi.org/10.1088/1751-8121/aaf3f0).
- [51] L. Canet, H. Chaté and B. Delamotte, *General framework of the non-perturbative Renormalization Group for non-equilibrium steady states*, J. Phys. A **44**(49), 495001 (2011).
- [52] M. Tarpin, *et al Relation between time and space Eulerian intermittency in Sabra shell model*, in preparation (2022).
- [53] D. Bandak, G. L. Eyink, A. Mailybaev and N. Goldenfeld, *Thermal noise competes with turbulent fluctuations below millimeter scales*, doi:[10.48550/ARXIV.2107.03184](https://doi.org/10.48550/ARXIV.2107.03184) (2021).
- [54] J. B. Bell, A. Nonaka, A. L. Garcia and G. Eyink, *Thermal fluctuations in the dissipation range of homogeneous isotropic turbulence*, Journal of Fluid Mechanics **939**, A12 (2022), doi:[10.1017/jfm.2022.188](https://doi.org/10.1017/jfm.2022.188).
- [55] R. M. McMullen, M. C. Krygier, J. R. Torczynski and M. A. Gallis, *Navier-Stokes equations do not describe the smallest scales of turbulence in gases*, Phys. Rev. Lett. **128**, 114501 (2022), doi:[10.1103/PhysRevLett.128.114501](https://doi.org/10.1103/PhysRevLett.128.114501).
- [56] L. Canet, B. Delamotte, D. Mouhanna and J. Vidal, *Optimization of the derivative expansion in the nonperturbative Renormalization Group*, Phys. Rev. D **67**, 065004 (2003), doi:[10.1103/PhysRevD.67.065004](https://doi.org/10.1103/PhysRevD.67.065004).
- [57] L. Canet, B. Delamotte, D. Mouhanna and J. Vidal, *Nonperturbative Renormalization Group approach to the Ising model: A derivative expansion at order  $\partial^4$* , Phys. Rev. B **68**, 064421 (2003), doi:[10.1103/PhysRevB.68.064421](https://doi.org/10.1103/PhysRevB.68.064421).